GEOLOGICA CARPATHICA, 2026, 77, 2, 95–113 https://doi.org/10.31577/GeolCarp.2026.05

Provenance and anthropogenic contamination of the Ventosa beach sediments in the Oaxaca State, Mexican Pacific

MAYLA A. RAMOS-VÁZQUEZ[1,2], JOHN S. ARMSTRONG-ALTRIN[3,✉] and SANJEET K. VERMA[1]

[1]División de Geociencias Aplicadas, Instituto Potosino de Investigación Científica y Tecnológica (IPICYT), Camino a la Presa San José 2055, San Luis Potosí 78216, México
[2]Present address: Instituto de Ingeniería, Universidad Nacional Autónoma de México, Ciudad Universitaria, Circuito Exterior S/N, Coyoacán 04510, México
[3]Universidad Nacional Autónoma de México, Instituto de Ciencias del Mar y Limnología, Unidad de Procesos Oceánicos y Costeros, Ciudad Universitaria, Ciudad de México 04510, México

(Manuscript received September 5, 2025; accepted in revised form February 25, 2026; Associate Editor: Katarína Bónová)

Abstract: Sediment geochemistry and 165 detrital zircon grains U–Pb ages are analyzed from the Ventosa beach sediments in the Gulf of Tehuantepec, Mexican Pacific. The objective is to investigate the sediment weathering condition, compositional variations, and to locate the source areas delivering sediments to the coast. Weathering indices reveal a moderate chemical weathering, indicating that the sediments are chemically immature. The SiO_2 content (~72–78 wt.%) and the trace element concentrations indicate that the beach sediments are dominantly derived from the felsic igneous rocks. The rare earth element (REE) patterns of the Ventosa sediments are homogeneous and are depleted relative to the average upper continental crust (UCC) values. The environmental indices reveal a "moderately severe enrichment" for Cu content (Enrichment Factor EF=5.62–8.87; and Geo Accumulation Index I_{geo}=1.41–1.98). Anthropogenic enrichment in Pb, Ba, and Zn contents with the possibility of adverse aquatic biota effect is also observed. Th/U ratios in zircon grains are >0.3, indicate an igneous origin. Two major U–Pb age groups are identified i.e. (1) Miocene (~23–12.9 Ma) and (2) Proterozoic (Neoproterozoic: ~999–545 Ma; Mesoproterozoic: ~2549–1006 Ma). These ages suggest that the zircon grains were originated from the nearby source terranes, most likely from the Cenozoic plutons exposed along the southern Oaxaca coastal region, as well as the volcanic and sedimentary rocks of the Todos Santos Formation.

Keywords: minerals, geochemistry, geochronology, coastal sediments

Introduction

In the fluvial environment, sediments may undergo chemical and physical changes during their transport from the source to sink (Tsanga et al. 2023; Bónová et al. 2024; Wu et al. 2025). Similarly, sediment composition has a strong spatial heterogeneity, and their sources may vary among different regions with respect to the geology of the area (Verma et al. 2016, 2017; Tawfik et al. 2018; Ayala-Pérez et al. 2021).

Provenance of sediments can be inferred through variations in the mineralogical and geochemical compositions (Ndjigui et al. 2014; Armstrong-Altrin et al. 2021; Andreasen et al. 2023; Elbakhouch et al. 2025). Other than provenance, trace element concentrations can also reveal the amount of heavy metal accumulation in sediments (Christophoridis et al. 2009; Wang et al. 2015; Kanwel et al. 2025; Pérez-Alvarado & Armstrong-Altrin 2025). In fact, the coastal sediments are widely studied to assess the environmental conditions, because of their contaminant storage capacity and resistance to biological degradation (De Falco et al. 2003; Ramos-Vázquez et al. 2018; Sopie et al. 2023; dos Santos et al. 2025).

Zircon grains occur in a variety of igneous rocks and preserves its primary properties, even after a lengthy geological process. Due to its chemical and thermal stabilities, zircon grains are reliable to study the past geological history (Zhou et al. 2021). Hence, determining zircon grains U–Pb ages is important to understand the sediment transport history and their parent rocks (Ramos-Vázquez & Armstrong-Altrin 2021; Aranda-Gómez et al. 2024; Chen et al. 2025). Detrital zircon grains have proven to preserve reliable information about the parent rocks and provide clues regarding variations in sediment provenance and depositional history (Moore et al. 2021; Sharman et al. 2021; Zhao et al. 2025).

Although, numerous studies demonstrated the importance of U–Pb geochronology in the Gulf of Mexico coastal sediments (Tapia-Fernández et al. 2017; Armstrong-Altrin 2020, 2024; Ramos-Vázquez 2023; Shukla et al. 2024, 2025), provenance studies based on the combination of sediment geochemistry and geochronology in the Mexican Pacific is inadequate.

This study examines the mineralogy and geochemistry of the Ventosa beach sediments, Gulf of Tehuantepec, Oaxaca State, Mexican Pacific. In addition, U–Pb ages of 165 zircon grains are also integrated with the geochemistry data. The objective is to evaluate the factors, which are controlling the sediment composition, to infer the weathering intensity, and to identify the probable source terranes delivering sediments to the

✉ corresponding author: John S. Armstrong-Altrin
armstrong@cmarl.unam.mx

Ventosa beach. Furthermore, the effect of anthropogenic activities in the beach sediments is also addressed in this study.

Study area

Twenty sediment samples were collected from the Ventosa beach at the Gulf of Tehuantepec, Mexican Pacific (Fig. 1; between 16°10'49.53"N, 95°9'27.45"W and 16°11'8.42"N, 95°9'12.75"W). The Gulf of Tehuantepec is in the southern region of the Mexican Pacific. The region is very productive and consists of a dynamic system, influenced by warm ocean currents with an average of 26 °C and an upwelling is induced by "Tehuanos" with an intense wind speed of 10–24 m/s from November to February (Hendy & Pedersen 2006; Fiedler & Lavín 2017; Ramos-Vázquez et al. 2024a, b). The coastal regions in the Oaxaca State are dominated by commercial fisheries with rapid growth in the urban industries. In the coastal region of the Oaxaca State, exploitation of Au, Cu, Pb, and Zn deposits is common, and the largest mine is San José, which is exploring Ag and Au since 1995 (Castillo-Nieto et al. 1996; Azamar Alonso & Tellez Ramirez 2021).

The discharge of waste materials from the construction of Trans-Isthmus highway and the Salina Cruz oil refinery system are highly influence the Gulf of Tehuantepec coastal pollution level (Botello et al. 1998). The sediment input to the Gulf of Tehuantepec is by the 240 km long Tehuantepec River (CONAGUA 2002; INEGI 2008) (Fig. 1). The Gulf of Tehuantepec coast is integrated with Mesozoic sedimentary (Ortega-Gutiérrez et al. 2018) and Quaternary alluvial soils mainly litharenite type (INEGI 2008). The Oaxacan and Mixtec terranes are composed of the metamorphic basements named as the Oaxacan and Xolapa Complexes, which are in contact with the Caltepec fault. The Oaxacan Complex constitutes a part of the Proterozoic basement in the southern Mexico. Additionally, the Mesoproterozoic microcontinent Oaxaquia consists of metasedimentary sequences as well as high-temperature pegmatites (Elizondo-Pacheco et al. 2025). Geochronological data revealed the exposure of Cretaceous rocks in the Puerto Vallarta batholith and Miocene rocks in the vicinity of Salina Cruz. In the Río Verde Batholith, the rocks are granitic to tonalitic composition of calc-alkaline affinities and associated with hornblende. The reported K–Ar geochronological ages are varying between 29 Ma and 23 Ma (Morán-Zenteno et al. 2018).

Methodology

Sampling

Twenty sediment samples, approximately 2 kg each, representing 500 m distance were taken from the Ventosa Beach, near to the mouth the Tehuantepec River, which approximately covered 5 km of the Gulf of Tehuantepec coast. The samples were dried for one day at 50 °C in the Sedimentology Laboratory, Instituto de Ciencias del Mar y Limnología (ICML), Universidad Nacional Autónoma de Mexico (UNAM). Samples were prepared for the identification of minerals in sediments, major, trace, and rare earth elements geochemical analysis, and for zircon grains U–Pb dating.

40 g of sediment samples were air-dried and powdered by an agate mortar for geochemical analysis. For U–Pb dating, 165 zircon grains were separated from two sediment samples (V1 and V2), because these two samples are enriched in zircon grains compared to other samples.

Modal components

10 thin-sections were prepared to count the modal components of sediments by following the method proposed by Gazzi-Dickinson (Dickinson 1970, 1985; Ingersoll et al. 1984; Suttner & Basu 1985). Totally 300 grains were counted. The framework grains counted are: total quartz [Qt = all quartz grains], total feldspar [(Ft) = K-feldspar (Fk) + plagioclase (P)], and total lithics [(Lt) = volcanic (Lv) + sedimentary (Ls) + metamorphic (Lm) + plutonic (Lp)], heavy minerals (HM), and biogenic components [(B) = shells, algae, and corals].

Mineralogy

The minerals in 10 sediment samples were determined by the PHILLIPS XL-30 Scanning Electron Microscope (SEM) equipped with EDAX spectrometer (EDS) system at University Laboratory of Petrology, Institute of Geophysics, UNAM, Mexico. Approximately, 15 g of sediment samples were utilized for the identification of minerals. Prior to analysis, ten 1-inch diameter circular coverslips were washed with acetone. Graphite double-sided tape was placed on one side of each coverslip, then even coverslip was introduced into a bag with sediment, where the material was retained on the tape. Next, the coverslips were coated with graphite using a graphite evaporator to increase the material's electrical conductivity (Girão et al. 2017).

Geochemistry

Major element concentrations

Major element concentrations for 10 samples (25 g) were analyzed. For the loss on ignition test, the powdered sediments were placed in a muffle furnace at 1000 °C for 2 h. Simultaneously, 25 g of powdered sediment was added to lithium tetraborate and heated to 1000 °C to form a fused sample. Calibration curves were prepared by using an International reference material and the standard JGB1 (GSJ), with an analytical accuracy of 5 % (Lozano & Bernal 2005).

Trace and rare earth element concentrations

The trace and REE were quantified in 10 sediment samples (12 g) by an Ultratrace – total acid digestion method using

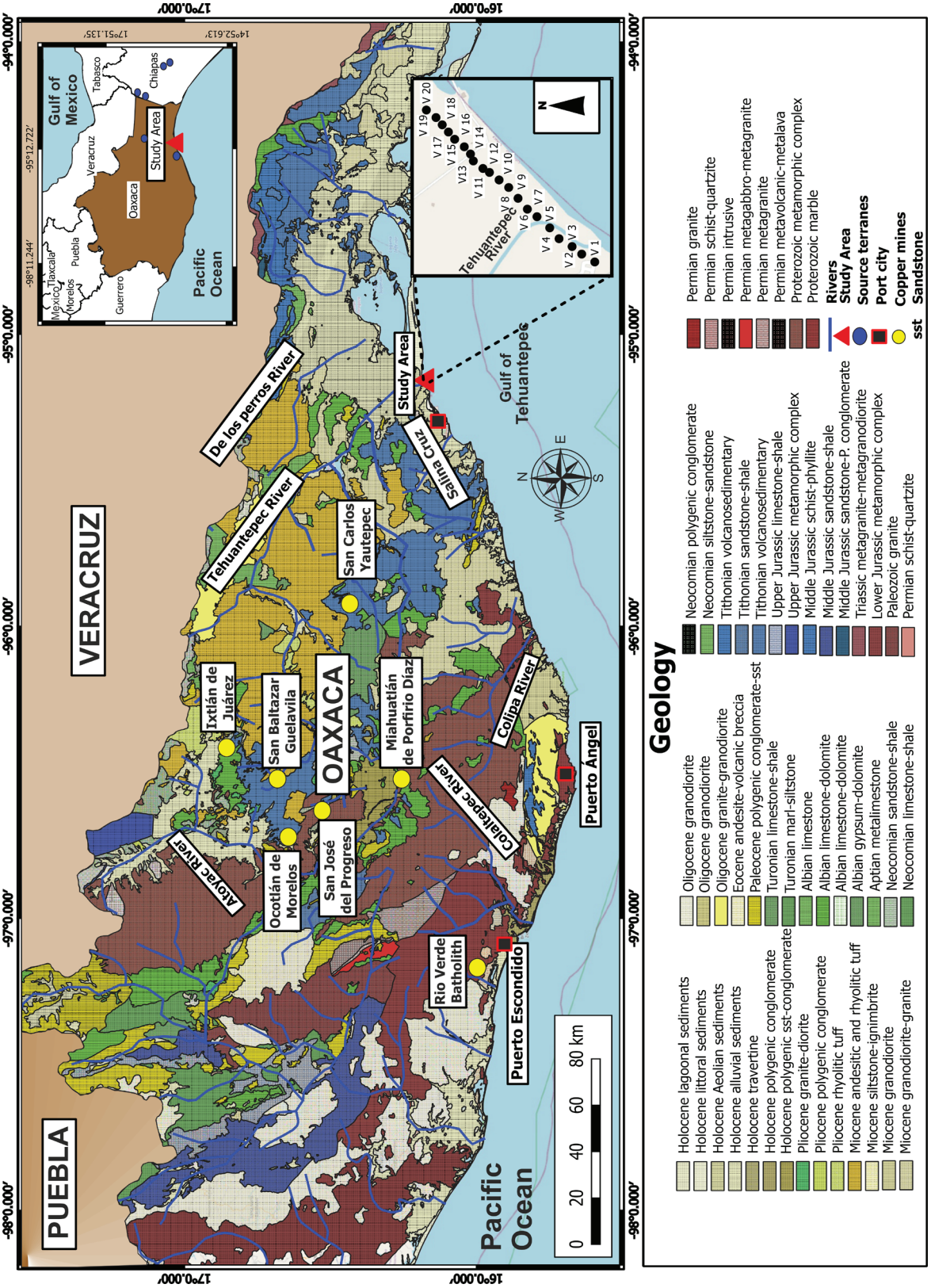

Fig. 1. Geological map showing sample locations (V1 to V20) in the Ventosa beach, Gulf of Tehuantepec, Oaxaca State, Mexican Pacific (source: Dirección General de Geografía del Territorio Nacional, 2025; scale 1:1,000,000).

an ICP-OES/ICP-MS at the Activation Laboratories Ltd., Canada (Leikin & Phillips 2023). All samples were determined twice with an analytical precision varying from 5 % to 10 %. The standard reference materials used were SY-2 (syenite CCRMP, Canada) and GSR-4 (sediment IGGE, China) (Imai et al. 1995).

U–Pb dating of zircon grains

Two sediment samples from the Ventosa beach were selected for geochronology (sample numbers V1 and V2). These two samples contain a greater number of zircon grains relative to other samples. The zircon grains were picked under a stereoscopic microscope without any consideration regarding color, shape, or size, then the zircon grains were mounted in an epoxy resin and polished for subsequent analysis.

Zircon U–Pb geochronology was performed by a Laser Ablation Inductively Coupled Plasma Mass Spectrometry (LA-ICPMS) at Laboratory of Isotopic Studies (LEI), Institute of Geosciences, UNAM. The reference standard zircon employed were 91,500 (1062 Ma; Wiedenbeck et al. 1995) and Plešovice zircon (337±1 Ma; Sláma et al. 2008), which run for 12 and 24 analyses, respectively. The reference standard for zircon grains REE data was NIST 610 and normalized with the Chondrite values of Taylor & McLennan (1985). The ISOPLOT 3.70 Software is utilized for the preparation of the Concordia and histograms (Ludwig 2003).

165 zircon grains were dated by applying the discordance filter of ca. 30 % for positive discordance and 5 % for negative discordance (Gehrels 2014). There are three processes that can induce normal discordance in zircon grains: (i) Loss of radiogenic lead, (ii) gain of excess uranium after primary crystallization, and (iii) incorporation of common lead (Andersen et al. 2019).

Results

Modal compositional data

The average quartz–feldspar–lithic fragment ratios for the Ventosa beach sediments are Qt_{68}–Ft_{6}–Lt_{26} (Table 1). The Ventosa sediments are dominated mostly by quartz (Qt) and plutonic (Lp) grains, probably represent granite as a primary source rock. Lithic fragments are composed of plutonic, volcanic, and sedimentary rock fragments, suggesting that the sediments were mostly derived from granites and recycled sedimentary rocks with a minor contribution from andesites.

Similarly, sediments are depleted in rock forming minerals such as plagioclase (P) and potash feldspar (Fk). The compositional maturity is revealed by the greater number of heavy minerals (HM) like zircon, rutile, magnetite, and apatite compared to other grains. These minerals may derive from felsic plutonic rocks (coastal batholith) and from sedimentary rocks exposed along the Mexican Pacific coast.

Mineralogy

The SEM images illustrating the size and morphology of sand grains are shown in Fig. 2A, B, and C, which are mostly sub-angular. In addition, mineral composition detected by SEM-EDS is shown in Fig. 3. SEM-EDS indicates an elevation in Si, K, Ca, Na, and Fe contents (Fig. 3A–E). These major oxides suggest the presence of various minerals, i.e. anorthite and albite (Fig. 3A), anorthite and magnetite (Fig. 3B), K-feldspar (Fig. 3C), magnetite (Fig. 3D), and quartz (Fig. 3E).

Bulk sediment geochemistry

The SiO_2 content varies from ~72 to 78 wt.% (Table 2). The average Al_2O_3 content is 8.86±0.96 (n=10). The major element concentrations are normalized against the average UCC values (Fig. 4A; Taylor & McLennan 1985). SiO_2 and K_2O contents are slightly higher, and remaining elements are lower than in UCC.

The trace element concentrations are reported in Table 3 and are normalized against UCC (Fig. 4B). In comparison with UCC the Cu, Ba, and Pb contents are enriched, and Zn content is depleted, except one sample. High field strength elements (HFSE) like Zr and Hf (7–10 ppm and 0.2–0.4 ppm) are lower than in UCC. The lithophile elements (LILE) like Ba, Rb, and Sr are varying from ~593 to 706 ppm, ~65.9 to 75 ppm, and ~185 to 243 ppm, respectively. The transitional trace elements (TTE) such as Cr, Co, V, and Ni are < 50 ppm, while Cu content is slightly enriched, which is > 50 ppm. The REE contents are reported in Table 3 and are normalized against the average chondrite values (Fig. 4C; Taylor & McLennan 1985). The REE patterns are enriched in light REE and are depleted in heavy REE contents (Fig. 4C). The Eu/Eu^*

Table 1: Modal compositional data for the Ventosa beach sediments, Gulf of Tehuantepec, Mexican Pacific.

Sample #	V1	V3	V5	V7	V9	V11	V13	V15	V17	V19
Qt	180	182	206	195	194	186	176	198	172	181
Fk	10	13	10	9	11	8	9	11	12	9
P	5	6	6	7	5	6	8	8	10	9
Lv	18	19	17	16	18	20	21	14	15	18
Ls	28	21	19	20	21	24	25	23	27	25
Lm	2	2	0	0	2	3	1	0	0	2
Lp	31	28	25	26	28	31	32	28	33	31
HM	26	28	17	26	21	22	28	17	30	25
B	0	1	0	1	0	0	0	1	1	0
n	300	300	300	300	300	300	300	300	300	300

Grain parameters: Qt=all quartz grains, Fk=K-feldspar, P=plagioclase, Lv=volcanic (basalt and andesite), Ls=sedimentary (limestone, sandstone, and shale), Lm=metamorphic (schist), Lp=plutonic (granite), HM=heavy minerals (zircon, rutile, magnetite, etc.), and B=biogenic components (shell, algae and coral fragments), n=number of grains counted.

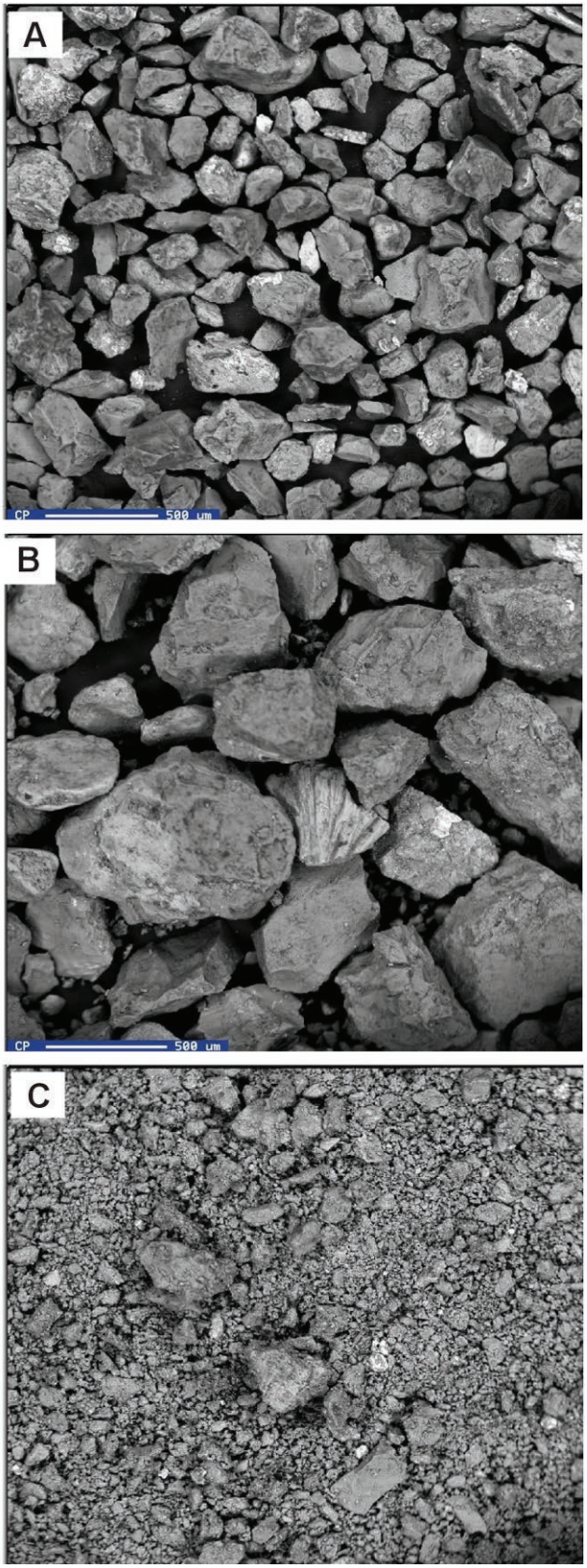

Fig. 2. (A), **(B)**, and **(C)** SEM-images showing general morphology of quartz grains in the Ventosa beach sediments.

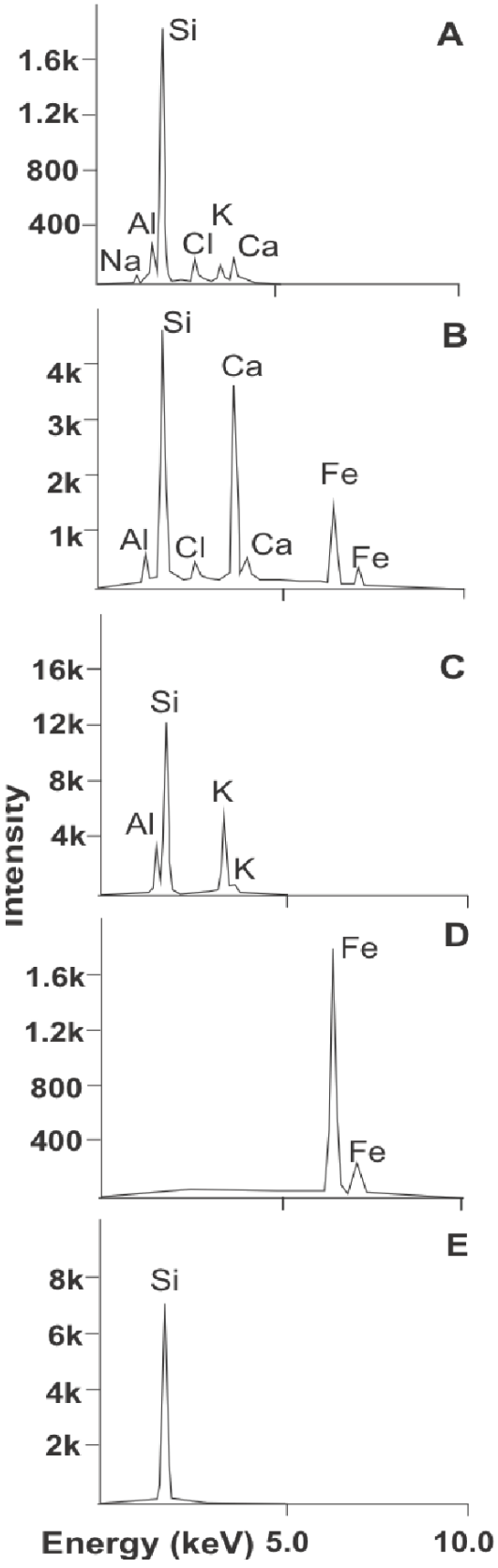

Fig. 3. SEM-EDS analysis for the beach sediments: **(A)** albite and anorthite, **(B)** anorthite and magnetite, **(C)** K-feldspar, **(D)** magnetite, and **(E)** quartz.

Table 2: Major element concentrations (wt.%) for the Ventosa beach sediments, Gulf of Tehuantepec, Mexican Pacific.

Sample	V1	V3	V5	V7	V9	V11	V13	V15	V17	V19
SiO_2	77.4	72.8	74.4	72.1	76.2	78.4	77.7	76.6	77.9	73.6
TiO_2	0.25	0.18	0.17	0.37	0.18	0.21	0.17	0.07	0.14	0.39
Al_2O_3	8.36	10.19	9.48	10.19	9.01	8.14	7.74	8.46	7.52	9.49
Fe_2O_3	1.63	3.32	2.27	3.85	2.21	1.49	1.29	2.79	2.35	4.02
MnO	0.03	0.02	0.02	0.04	0.02	0.03	0.02	0.01	0.02	0.05
MgO	1.03	1.02	1.02	1.04	1.02	1.03	1.02	1.01	1.02	1.05
CaO	2.52	2.25	2.45	2.34	2.25	2.21	3.05	1.79	3.20	2.72
Na_2O	2.95	3.20	2.96	3.10	2.72	2.45	2.75	2.61	2.73	2.60
K_2O	3.78	4.32	4.15	4.12	4.16	3.90	3.83	4.42	3.65	3.69
P_2O_5	0.07	0.07	0.06	0.07	0.06	0.05	0.05	0.04	0.05	0.08
LOI	1.52	2.20	2.19	2.04	1.42	1.38	1.63	1.44	1.39	1.52
Sum	99.6	99.6	99.2	99.2	99.2	99.3	99.3	99.3	99.9	99.2
CIA	47.5	51.1	49.8	51.6	49.7	48.7	44.6	49	44	51.3
PIA	45.6	51.8	49.6	52.8	49.4	47.6	40.3	47.9	39.5	52.1
CIW	60.4	65.2	63.7	65.2	64.4	63.6	57.2	65.8	55.9	64
ICV	1.50	1.40	1.37	1.45	1.39	1.39	1.57	1.50	1.74	1.53
SiO_2/Al_2O_3	9.26	7.15	7.85	7.07	8.45	9.63	10.04	9.06	10.36	7.75
K_2O/Na_2O	1.28	1.35	1.40	1.33	1.53	1.59	1.39	1.70	1.33	1.42
Al_2O_3/Na_2O	2.84	3.19	3.20	3.29	3.31	3.32	2.81	3.24	2.75	3.64
K_2O/Al_2O_3	0.45	0.42	0.44	0.40	0.46	0.48	0.49	0.52	0.49	0.39

Chemical Index of Alteration (CIA=$[Al_2O_3/(Al_2O_3+CaO^*+Na_2O+K_2O)]\times100$; Nesbitt & Young 1982), Chemical Index of Weathering (CIW=$[Al_2O_3/(Al_2O_3+CaO^*+Na_2O)]\times100$; Harnois 1988), PIA Plagioclase Index of Alteration ($[Al_2O_3-K_2O/(Al_2O_3+CaO^*+Na_2O)]\times100$; Fedo et al. 1995), ICV Index of Compositional Variability ($[(CaO+K_2O+Na_2O+Fe_2O_3(t)+MgO+MnO+TiO_2)/Al_2O_3]$; Cox et al. (1995), $Fe_2O_3^*$ total Fe expressed as Fe_2O_3.

ratio values vary between 0.7 and 1.1 (Table 3). The variations in total REE content among ten samples are poor.

Zircon geochronology

The age distribution is illustrated in Fig. 5 A, B, C, and D, and the U–Pb ages are reported in the Supplementary Table S1. 20 out of 165 lies on bright homogenous zircon grains with an isomeric or elliptical shape (Fig. 5A and C). 145 zircon grains are with concordant values, which provided two principal age populations. The minor age population group varies between 13 Ma and 31 Ma with the domination of Cenozoic zircon grains. However, the predominant U–Pb ages represent Miocene (n=56) and Oligocene (n=5). Another principal age population group ranges between 545–2549 Ma (Neoproterozoic–Paleoproterozoic; sample V2) and 657–1499 Ma (Neoproterozoic–Mesoproterozoic; sample V1). A dominant peak at 1000 Ma and a subordinate peak at 1110 Ma are identified.

The distribution of age populations between samples V1 and V2 is, i.e. Cenozoic (number of grains n=28 and 33, respectively), Mesozoic (n=3 and 7, respectively), Paleozoic (n=1 and 11, respectively), and Proterozoic (n=68 and 14, respectively). In fact, a variation in the distribution of age populations between samples V1 and V2 is identified. For example, the differences in the distribution of Cenozoic (n=28 and 33, respectively) and Mesozoic (n=3 and 7, respectively) grains is not significant. However, a significant difference in the number of zircon grains for the Paleozoic (n=1 and 11 for V1 and V2), and Proterozoic (n=68 and 14 for V1 and V2, respectively) is noted. The probability density plot shows high peak at Proterozoic (50 %) and Cenozoic (37 %) (Fig. 5B and D).

REE patterns of zircon grains

The trace element contents of zircon grains are reported in the Supplementary Table S2. The chondrite normalized REE plots are enriched in HREE (La/Yb=0.004 (V1) and 0.07 (V2)) with positive Ce and negative Eu anomalies. A positive Ce (Ce/Ce^*=1.16–334 and 1.18–206 in V1 and V2, respectively) and negative Eu anomalies (Eu/Eu^*=0.01–1.08 (V1) and 0.02–0.64 (V2)) are characteristic of magmatic origin (Fig. 6A–G) (Zhao et al. 2025). The REE patterns between samples V1 and V2 are similar. However, a wide variation in the europium anomaly is noted among zircon grains. For instance, in sample V1, the Eu/Eu^* ratio values for zircon grains are mostly negative and less than 1. On the other hand, it is near to 1 for a few zircon grains belong to Neoproterozoic and Mesoproterozoic ages (Fig. 6C). Among Mesozoic there are differences with respect to the intensity of the europium anomaly, i.e. it is more negative for the Cretaceous than Triassic. Similarly, absence of negative europium anomaly is noted in some zircon grains belong to Paleozoic (Devonian and Permian) and Proterozoic (Paleoproterozoic and Neoproterozoic) (Fig. 6F and G).

Although positive Ce anomaly is common in all ages, the absence of anomaly is observed in a few Miocene and Neoproterozoic zircon grains (Fig. 6D and G). It seems that the variations in REE patterns among zircon grains with respect to their age reveals a diversity in their source. In addition, the REE geochemistry of Devonian zircon grains of this

study is compared with the published data from the Gulf of Mexico (GoM) and Mexican Pacific (MP) beach areas. This comparison suggests a similarity in the REE patterns among the Devonian zircon grains, especially in the positive cerium and negative europium anomalies (Fig. 7).

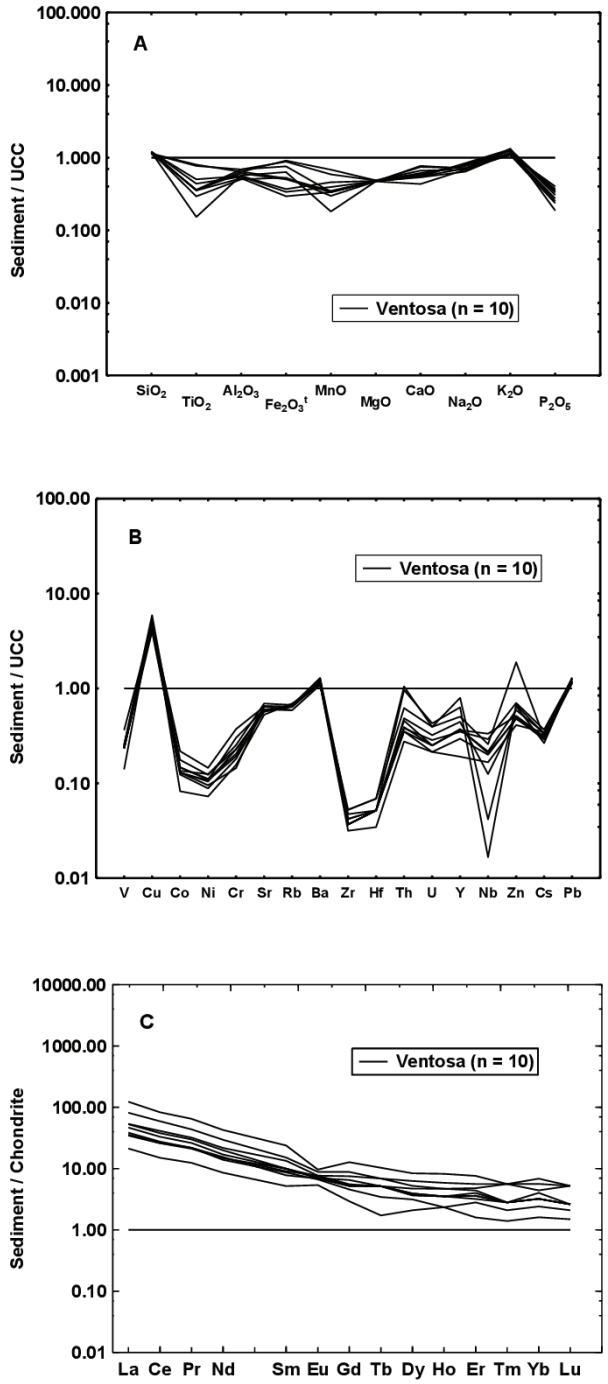

Fig. 4. (A) Major element concentrations of the Ventosa beach sediments normalized against average upper continental crust values (Taylor & McLennan 1985). **(B)** Trace element concentrations of the Ventosa sediments normalized against average upper continental crust values. **(C)** Chondrite-normalized REE patterns for the Ventosa beach sediments.

Discussion

Elemental variations

Correlation coefficient values are useful to infer the variations in the bulk composition of sediments (Madhavaraju et al. 2024). An inter elemental correlation between major and trace elements can indicate the association of minerals in sediments (Wang et al. 2019; Hossain et al. 2025; Kasanzu 2025). The correlation coefficient values are reported in the Supplementary Table S3. The negative correlation between SiO_2 versus Al_2O_3, Fe_2O_3, Na_2O, and Sr in the beach sediments suggests that these elements are not associated with aluminosilicates (−0.96, −0.85, −0.64, and −0.84, respectively; $p<0.05$; $n=10$). The correlation of Al_2O_3 versus Fe_2O_3, P_2O_5, and Sr ($r=0.74$, 0.63, and 0.80, respectively, $n=10$) is significant, indicating an association of Fe with aluminosilicates (Windom et al. 1989; Djibril et al. 2024). A significant correlation of ∑REE against Ni and Mn contents suggests the abundance of minerals like magnetite in sediments. The ∑REE content shows a significant correlation against Th, U, V, and Y ($r=0.95$, 0.78, 0.92, and 0.96, respectively; $n=10$), while a week correlation against Al_2O_3 ($r=0.32$) reveals that REEs are associated with accessory minerals rather than aluminosilicates (Chougong et al. 2021; Janpou et al. 2024). A strong positive correlation observed between ∑REE and other elements (Ti, Mn, Mg, P, Co, Cr, Hf, Zr, Th, U, and Y) indicates their association with secondary mineral phases such as clay, phosphate and Fe–Mn oxides, and heavy minerals like rutile, apatite, and zircon (Sai Babu et al. 2024). In addition, a positive correlation for LREE against P_2O_5 content indicates the concentration of apatite in sediments (Hermann & Rubatto 2009).

Sediment contamination

Rivers are considered as a major agent of transporting sediments from the land to the sea and are also rich in potentially toxic elements (Flores-Castro & Armstrong-Altrin 2022; Felicio dos Santos et al. 2025; Flores-Ocampo et al. 2025; Islam et al. 2025). To evaluate the metal enrichment in sediments and to differentiate the natural and anthropogenic sources, we utilized several environmental indices like Enrichment Factor (EF; Zoller et al. 1974), Geo-accumulation index (I_{geo}; Müller 1969), Pollution Load Index (PLI; Tomlinson et al. 1980), and Potential Ecological Risk Index (PERI: Håkanson 1980) (Table 4). The procedures applied to calculate these indices are provided in the Supplementary file.

The EF indicates that Cu has the highest value, which vary between 5.62 and 8.87, suggesting moderately severe enrichment (Table 5). The second and third places are for Pb and Ba contents (~1.47–2.07 and ~1.58–1.83, respectively), which reveal no enrichment. The elements with low EF values (<0.5) are Co and Ni (0.13–0.33 and 0.12–0.22, respectively). The I_{geo} values for Ni (−4.37 to −3.37), Co (−4.19 to −2.78), and Cr (−3.38 to −2.01) are negative. The Cu concentration shows values between 1.41 and 1.98 that indicate Class 2 and

Table 3: Trace and rare earth element concentrations (in ppm) for the Ventosa beach sediments.

	V1	V3	V5	V7	V9	V11	V13	V15	V17	V19
Ba	593	705	683	706	647	630	658	610	614	598
Co	2.5	2.5	2.2	3	2.1	2.2	2.2	1.4	2.3	3.7
Cr	25	17	12	21	15	19	16	13	19	31
Cs	1.39	1.69	1.56	1.52	1.43	1.35	1.4	1.59	1.33	1.22
Cu	148	124	99.7	114	108	137	121	139	114	118
Hf	0.4	0.3	0.3	0.3	0.3	0.3	0.3	0.2	0.3	0.4
Mo	0.75	0.45	0.4	0.29	0.32	0.32	0.41	0.31	0.35	0.34
Nb	3.1	3.5	2.6	0.2	4	1.5	2.5	2	2.4	0.5
Ni	4.8	4.9	4.2	5.4	3.9	4.6	4.7	3.2	5.5	6.4
Pb	21.8	21.6	20.2	20.2	19.3	22.1	19.4	20.7	20.1	21.4
Rb	65.9	72.2	71.7	75	72.4	71.6	73.2	77.6	73.3	66.1
Sn	8	9	9	8	10	12	10	14	12	10
Sr	211	226	229	243	207	199	201	185	205	225
Th	6.5	4	3.7	10.1	4.1	5.1	4.8	2.9	3.7	11
U	1.1	0.8	0.7	1.2	0.7	0.9	0.7	0.6	0.6	1.1
V	27	26	25	36	25	27	26	15	25	39
Y	11.1	7.7	8.1	13.9	8	9.8	8.2	4.2	6.5	17.5
Zn	134	50	42	47.7	36.5	35.4	33.9	29.2	34.5	46.1
Zr	10	7	7	9	8	8	7	6	7	10
V/Cr	1.1	1.5	2.1	1.7	1.7	1.4	1.6	1.2	1.3	1.3
Ni/Co	1.9	2.0	1.9	1.8	1.9	2.1	2.1	2.3	2.4	1.7
Cu/Zn	1.1	2.5	2.4	2.4	3.0	3.9	3.6	4.8	3.3	2.6
La	19.7	13.1	12.7	30	13	19.4	17.2	7.8	14.2	45.1
Ce	39.4	25.5	24.9	56.9	25	36.3	31.7	14.4	26.4	79.6
Pr	4.4	3	2.9	6	3	4.1	3.6	1.7	3	8.9
Nd	15.5	10.7	10.5	21	11	14.2	12.1	6.1	9.9	30.4
Sm	3.1	2.1	2.3	3.5	1.8	2.3	2.3	1.2	2	5.5
Eu	0.67	0.67	0.65	0.77	0.6	0.61	0.61	0.47	0.58	0.84
Gd	2.3	1.7	1.6	2.7	1.6	2	1.6	0.9	1.4	3.9
Tb	0.4	0.3	0.3	0.4	0.3	0.3	0.3	0.1	0.2	0.6
Dy	2	1.5	1.4	2.4	1.5	1.8	1.4	0.8	1.2	3.2
Ho	0.4	0.3	0.3	0.5	0.3	0.4	0.3	0.2	0.2	0.7
Er	1.2	0.9	0.8	1.4	1	1.1	0.9	0.4	0.7	1.9
Tm	0.2	0.1	0.1	0.2	0.1	0.1	0.1	<0.1	<0.1	0.2
Yb	1.1	0.8	0.8	1.4	0.8	1	0.8	0.4	0.6	1.7
Lu	0.2	0.1	0.1	0.2	0.1	0.1	0.1	<0.1	<0.1	0.2
LREE	82.1	54.4	53.3	117.4	53.8	76.3	66.9	31.2	55.5	169.5
HREE	7.8	5.7	5.4	9.2	5.7	6.8	5.5	2.8	4.3	12.4
Eu/Eu*	0.7	1.1	1.0	0.7	1.1	0.9	0.9	1.1	1.0	0.5

LREE=La, Ce, Pr, Nd, and Pm; HREE=Tb, Dy, Ho, Er, Tm, Yb, and Lu; $Eu/Eu^{*}=Eu_{CN}/[(Sm_{CN})(Gd_{CN})]^{1/2}$; $_{CN}$= Chondrite normalized value (Taylor & McLennan 1985).

moderately contaminated (Table 6). On the other hand, PLI values for the Ventosa sediments are <1 (~0.39–0.61; Table 7), suggesting an absence of anthropogenic influence.

The Potential Ecological Risk Index (PERI) values for the transition metals Pb, Cu, Ni, Cr, and Zn are varying between 27.2 and 39.1, which implies a low ecological risk (Table 8). The concentration of the potentially toxic elements used to assess the anthropogenic source is in the order Cu>Pb>Zn>Ba. However, Cu is the only metal that falls under the category moderately severe enrichment.

Copper mines are common in the Mexican Pacific coast, especially in the Xolapa Complex (SGM 2021). The areas with high Cu deposits are in the south of Ocotlán de Morelos, Miahuatlán de Porfirio Díaz, San Baltazar Guelavila, and San Carlos Yautepec (Fig. 1). Similarly, the polymetallic Pb–Zn–Ag deposits are distributed in the eastern side of the Ixtlán de Juárez terrane (Fig. 1). Therefore, sediments derived from these areas naturally increase the Cu, Pb, and Zn contents in the Ventosa coastal sediments relative to UCC (CRM 1996; SGM 2021).

Weathering and sediment provenance

The weathering indices like CIA (Nesbitt & Young 1982), PIA (Fedo et al. 1995), and CIW (Harnois 1988) indicate moderate weathering in the source region (~44–52, ~40–53, and ~56–66, respectively) (Table 2). In addition, the ICV (Cox et al. 1995) values >1 (~1.4–1.6) indicate a moderate sediment maturity.

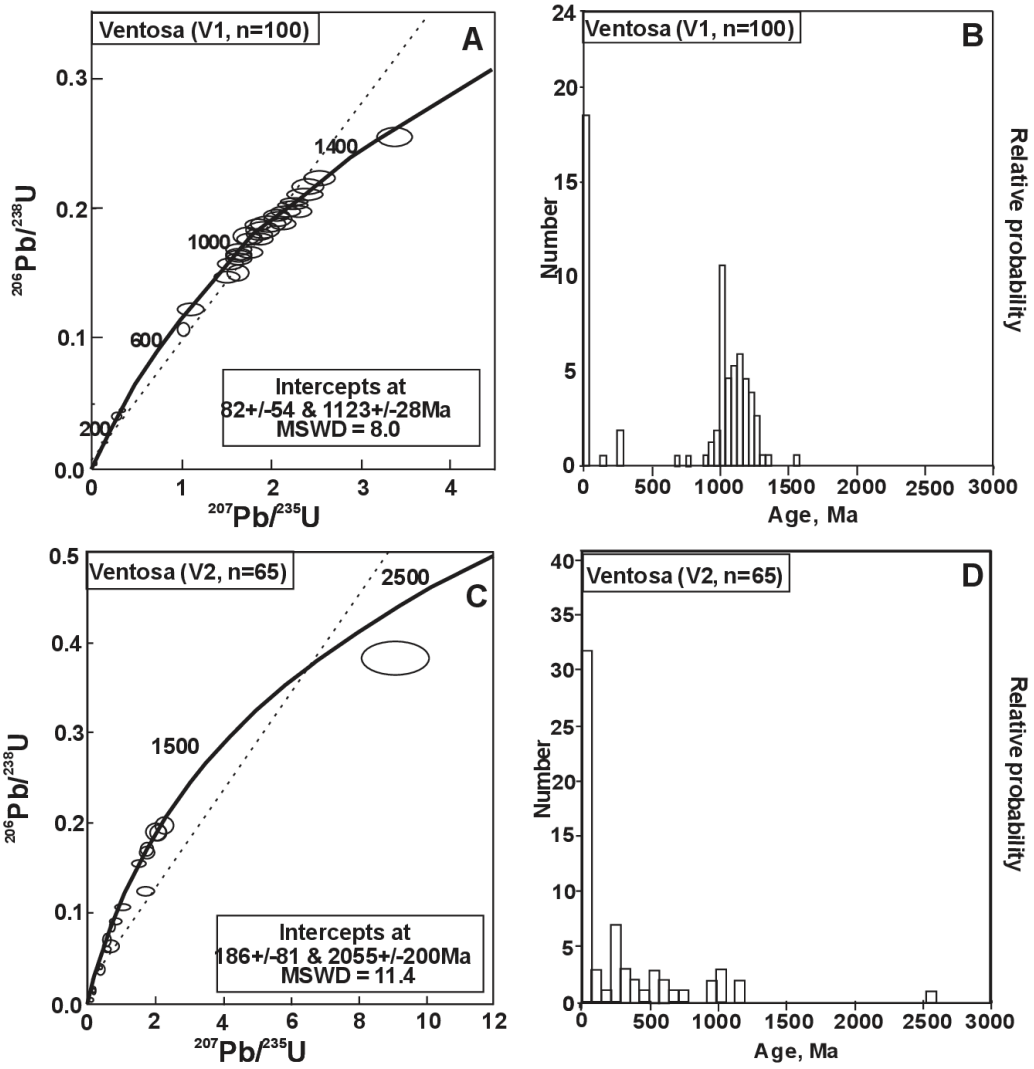

Fig. 5. U/Pb Concordia diagrams of the detrital zircon grains recovered from the Ventosa beach sediments (**A** and **C**) and histograms showing relative age probability distribution (**B** and **D**).

The Roser & Korsch (1988) diagram is widely utilized by numerous authors to differentiate the sediment provenance (Bahr & Keighley 2021; Ramos-Vázquez 2021; Pauli de Castro et al. 2023). This diagram indicates a felsic provenance for the Ventosa beach sediments (Fig. 8A). Similarly, a relationship between Ni and V contents observed in the Ni–Th*10–V plot also indicating a felsic source (Fig. 8B; Bracciali et al. 2007). Similarly, except three samples, the REE patterns of the Ventosa beach sediments are with a negative Eu anomaly (Eu/Eu^{*}=<1; Table 3), indicating their origin mostly from the felsic igneous rocks (Fig. 4C). This interpretation is consistent with the Qt_{68}–Ft_{6}–L_{26} ratio.

Implications based on zircon chemistry

The Th/U ratio in samples V1 and V2 varies between 0.05–1.12 and 0.05–1.0, respectively. Previous studies documented that Th/U ratio in igneous zircons is > 0.3, whereas it is <0.1 in metamorphic zircons (Zhao et al. 2025). In this study, most of the zircon grains have Th/U ratio values >0.3, suggesting an igneous origin (Fig. 8C). Belousova et al. (2002) and Grimes et al. (2007) proposed bivariate diagrams to evaluate the zircon origin, which are based on the U, Yb, Hf, and Y concentrations. Two bivariate diagrams based on these trace elements are plotted to infer the origin of zircon grains (Fig. 9A and B; Y vs. U and Hf vs. Y; respectively). These diagrams indicate that the zircon grains were mostly derived from the felsic igneous rocks.

U/Yb ratios of zircon grains vary between ~0.17–11.30 (V1) and ~0.36–3.89 (V2), which reflect a variation in the composition of melt at the time of crystallization. The average U/Yb ratios of zircon grains in V1 and V2 are like the continental granitoids and bulk continental crust (1.58 and 0.6, respectively). However, very high U/Pb ratios are related to zircon grains extracted from an arc source (Grimes et al. 2007). U/Yb ratio value is 1.7 for continental granitoids (Grimes et al.

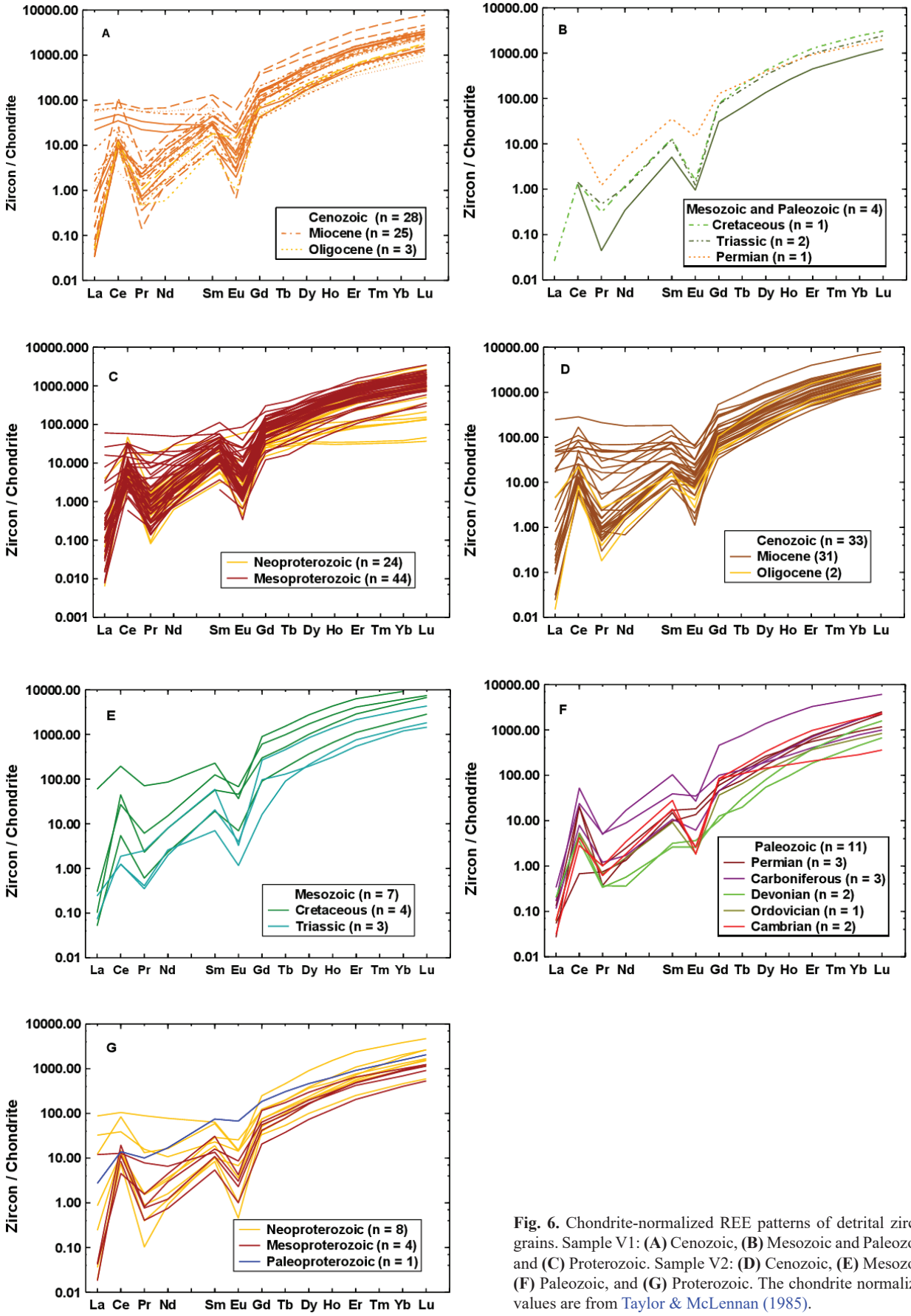

Fig. 6. Chondrite-normalized REE patterns of detrital zircon grains. Sample V1: **(A)** Cenozoic, **(B)** Mesozoic and Paleozoic, and **(C)** Proterozoic. Sample V2: **(D)** Cenozoic, **(E)** Mesozoic, **(F)** Paleozoic, and **(G)** Proterozoic. The chondrite normalized values are from Taylor & McLennan (1985).

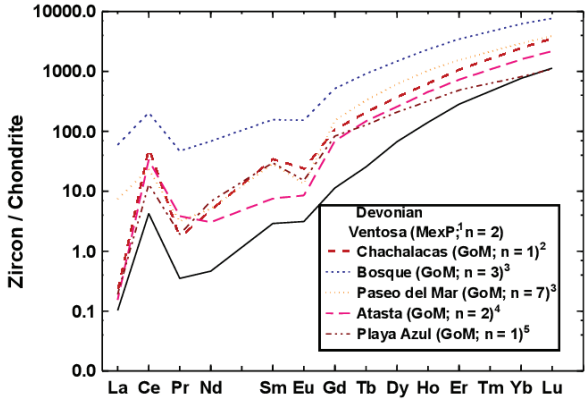

Fig. 7. Comparison of chondrite normalized rare earth element patterns of the Devonian zircon grains of this study with other similar studies. [1]This study; [2]Armstrong-Altrin et al. (2021); [3]Ramos-Vázquez & Armstrong-Altrin (2019); [4]Armstrong-Altrin et al. (2018); [5]Armstrong-Altrin (2024). MexP=Mexican Pacific; GoM=Gulf of Mexico; n=number of zircon grains. The chondrite normalized values are from Taylor & McLennan (1985).

2007), 2.1 for kimberlites (Farmer 2003), and 0.7 for the bulk continental crust (Rudnick & Gao 2003). In addition, on the U–Yb and U/Yb–Hf plots, zircon grains are plotted in the continental crust field (Fig. 9C and D; Grimes et al. 2007). This suggests continental crustal origin for the zircon grains. These observations reveal that the Ventosa beach sediments are composed of detritus derived from the nearby source rocks, exposed in the Oaxaca and Chiapas States. A detail about the potential source terranes from the Oaxaca and Chiapas States are provided in the following section.

Potential source terranes

The U–Pb ages of zircon grains in sample V1 represent two groups: (1) Cenozoic (~13–31 Ma), represented mostly by Miocene grains and (2) Proterozoic (~657–1499 Ma) principally by Mesoproterozoic. However, sample V2 is represented largely by Cenozoic (~14–31 Ma) with the domination of Miocene grains. A sub-ordinate peak is identified at 1110 Ma.

Table 4: Equations of environmental indices utilized in this study.

Index	Equation	Classification	Degree of Contamination	References
Enrichment Factor (EF)	$FE = \frac{(x/Al)_{sediment}}{(x/Al)_{reference}}$	Class 1 (1–2) Class 2 (2–3) Class 3 (3–5) Class 4 (5–10) Class 5 (10–25) Class 6 (25–50) Class 7 (>50)	1: no enrichment 2: minor enrichment 3: moderate enrichment 4: moderately severe enrichment 5: severe enrichment 6: very severe enrichment 7: extremely severe enrichment	Zoller et al. (1974)
Geo-accumulation index (I_{geo})	$I_{geo} = log\frac{M_i}{1.5M_r}$	Class 0 (I_{geo}=<0), Class 1 (0<I_{geo}<1) Class 2 (1<I_{geo}<2) Class 3 (2<I_{geo}<3) Class 4 (3<I_{geo}<4) Class 5 (4<I_{geo}<5)	0: practically uncontaminated 1: uncontaminated to moderately contaminated 2: moderately contaminated), 3: moderately to highly contaminated 4: highly contaminated 5: highly to extremely contaminated.	Müller (1969)
Pollution Load Index (PLI)	$PLI[(CF_1 \times CF_2 \times CF_3 \times CF_4 \times \ldots \times CF_n)1/n]$ $CF = M_{sediment}/M_{reference}$	PLI > 1	Progressive deterioration	Tomlinson et al. (1980)
Potential Ecological Risk Index (PERI)	$PERI = \sum_{i=1}^{n} EI$ $EI = T_i \times PI_i$ $PI_i = M_{sediment}/M_{reference}$	1) PERI <70 2) 70 PERI <140 3) 140 PERI <280 4) 280< PERI	1) low ecological risk, 2) moderate ecological risk, 3) considerable ecological risk, 4) very high ecological risk.	Håkanson (1980)

Table 5: Enrichment Factor (EF; Zoller et al. 1974) for the Ventosa beach sediments, Gulf of Tehuantepec.

Sample	Ba	Co	Cr	Cu	Ni	Pb	Sr	Zn	V
V1	1.61	0.22	0.45	8.85	0.16	1.92	0.90	2.82	0.38
V3	1.64	0.19	0.26	6.35	0.14	1.63	0.83	0.90	0.31
V5	1.75	0.18	0.20	5.62	0.13	1.67	0.92	0.83	0.33
V7	1.58	0.22	0.31	5.62	0.15	1.47	0.86	0.83	0.41
V9	1.69	0.18	0.26	6.22	0.13	1.64	0.85	0.74	0.34
V11	1.83	0.21	0.37	8.74	0.17	2.07	0.91	0.80	0.40
V13	1.81	0.20	0.29	7.31	0.16	1.72	0.87	0.72	0.37
V15	1.77	0.13	0.25	8.87	0.12	1.94	0.84	0.66	0.22
V17	1.79	0.22	0.37	7.32	0.20	1.90	0.94	0.78	0.37
V19	1.62	0.33	0.56	7.05	0.22	1.88	0.96	0.97	0.54
Avg.	1.71	0.21	0.33	7.20	0.16	1.78	0.89	1.00	0.37
Std. Dev.	0.09	0.05	0.11	1.27	0.03	0.19	0.04	0.64	0.08

Table 6: Geo-accumulation index (I_{geo}; Müller 1969) calculated based on Upper Continental Crust (UCC; Taylor & McLennan 1985) as background value for the Ventosa beach sediments, Gulf of Tehuantepec.

Sample	Ba	Co	Cr	Cu	Ni	Pb	Sr	Zn	V
V1	−0.48	−3.35	−2.32	1.98	−3.78	−0.23	−1.32	0.33	−2.57
V3	−0.23	−3.35	−2.87	1.73	−3.75	−0.24	−1.22	−1.09	−2.63
V5	−0.27	−3.53	−3.38	1.41	−3.97	−0.34	−1.20	−1.34	−2.68
V7	−0.22	−3.09	−2.57	1.60	−3.61	−0.34	−1.11	−1.16	−2.16
V9	−0.35	−3.60	−3.05	1.53	−4.08	−0.40	−1.34	−1.54	−2.68
V11	−0.39	−3.53	−2.71	1.87	−3.84	−0.21	−1.40	−1.59	−2.57
V13	−0.33	−3.53	−2.96	1.69	−3.81	−0.39	−1.39	−1.65	−2.63
V15	−0.44	−4.19	−3.26	1.89	−4.37	−0.30	−1.50	−1.87	−3.42
V17	−0.43	−3.47	−2.71	1.60	−3.58	−0.34	−1.36	−1.63	−2.68
V19	−0.46	−2.78	−2.01	1.65	−3.37	−0.25	−1.22	−1.21	−2.04
Avg.	−0.36	−3.44	−2.78	1.70	−3.82	−0.30	−1.31	−1.27	−2.61
Std. Dev.	0.09	0.36	0.42	0.18	0.28	0.07	0.12	0.62	0.37

Table 7: Pollution load indices (PLI; Tomlinson et al. 1980) calculated based on the upper continental crust (UCC; Taylor & McLennan 1985) as background value for the Ventosa beach sediments, Gulf of Tehuantepec.

Sample	CF_{Ba}	CF_{Co}	CF_{Cr}	CF_{Cu}	CF_{Ni}	CF_{Pb}	CF_{Sr}	CF_{Zn}	CF_{V}	PLI
V1	1.078	0.147	0.301	5.920	0.109	1.282	0.603	1.887	0.252	0.608
V3	1.282	0.147	0.205	4.960	0.111	1.271	0.646	0.704	0.243	0.524
V5	1.242	0.129	0.145	3.988	0.095	1.188	0.654	0.592	0.234	0.462
V7	1.284	0.176	0.253	4.560	0.123	1.188	0.694	0.672	0.336	0.566
V9	1.176	0.124	0.181	4.320	0.089	1.135	0.591	0.514	0.234	0.453
V11	1.145	0.129	0.229	5.480	0.105	1.300	0.569	0.499	0.252	0.496
V13	1.196	0.129	0.193	4.840	0.107	1.141	0.574	0.477	0.243	0.472
V15	1.109	0.082	0.157	5.560	0.073	1.218	0.529	0.411	0.140	0.391
V17	1.116	0.135	0.229	4.560	0.125	1.182	0.586	0.486	0.234	0.487
V19	1.087	0.218	0.373	4.720	0.145	1.259	0.643	0.649	0.364	0.610
Avg.	1.172	0.142	0.227	4.891	0.108	1.216	0.609	0.689	0.253	0.507
Std. Dev	0.077	0.036	0.069	0.601	0.020	0.059	0.049	0.432	0.061	0.070

Table 8: The Potential Ecological Risk (PERI; Håkanson 1980) calculated based on the upper continental crust (UCC; Taylor & McLennan 1985) as background value for the Ventosa beach sediments, Gulf of Tehuantepec.

Sample	PI Cr	PI Cu	PI Ni	PI Pb	PI Zn	EI Cr	EI Cu	EI Ni	EI Pb	EI Zn	PERI
V1	0.30	5.92	0.11	1.28	1.89	0.60	29.60	0.55	6.41	1.89	39.05
V3	0.20	4.96	0.11	1.27	0.70	0.41	24.80	0.56	6.35	0.70	32.82
V5	0.14	3.99	0.10	1.19	0.59	0.29	19.94	0.48	5.94	0.59	27.24
V7	0.25	4.56	0.12	1.19	0.67	0.51	22.80	0.61	5.94	0.67	30.53
V9	0.18	4.32	0.09	1.14	0.51	0.36	21.60	0.44	5.68	0.51	28.60
V11	0.23	5.48	0.10	1.30	0.50	0.46	27.40	0.52	6.50	0.50	35.38
V13	0.19	4.84	0.11	1.14	0.48	0.39	24.20	0.53	5.71	0.48	31.30
V15	0.16	5.56	0.07	1.22	0.41	0.31	27.80	0.36	6.09	0.41	34.98
V17	0.23	4.56	0.13	1.18	0.49	0.46	22.80	0.63	5.91	0.49	30.28
V19	0.37	4.72	0.15	1.26	0.65	0.75	23.60	0.73	6.29	0.65	32.02
Avg.	0.23	4.89	0.11	1.22	0.69	0.45	24.45	0.54	6.08	0.69	32.22
Std. Dev	0.07	0.60	0.02	0.06	0.43	0.14	3.00	0.10	0.29	0.43	3.50

The principal reason for the age difference between V1 and V2, especially the domination of Proterozoic grains in V1 is probably due to its location, which is near to the mouth of the Tehuantepec River.

The possible source terranes in the southern Mexico are briefly discussed below (refer Figs. 1 and 10 for locations). Weber et al. (2008) reported ages between 1.1 Ga and 920 Ma for zircon grains dated from sandstones in the Santa Rosa Formation, Chiapas Massif Complex. The granulite-bearing basement rocks of the Oaxaca terrane (The Oaxaca Complex) is made up of para- and orthogneisses. The protolith U–Pb zircon grain ages of these Oaxaca basement rocks are ranging from ~1000 Ma to 1300 Ma (Elizondo-Pacheco et al. 2025) and from ~820 Ma to 1600 Ma (Mesoproterozoic; Weber et al. 2006). In addition, Pindell et al. (2023) dated zircon grains recovered from the fluvial/alluvial fan deposits, as well as

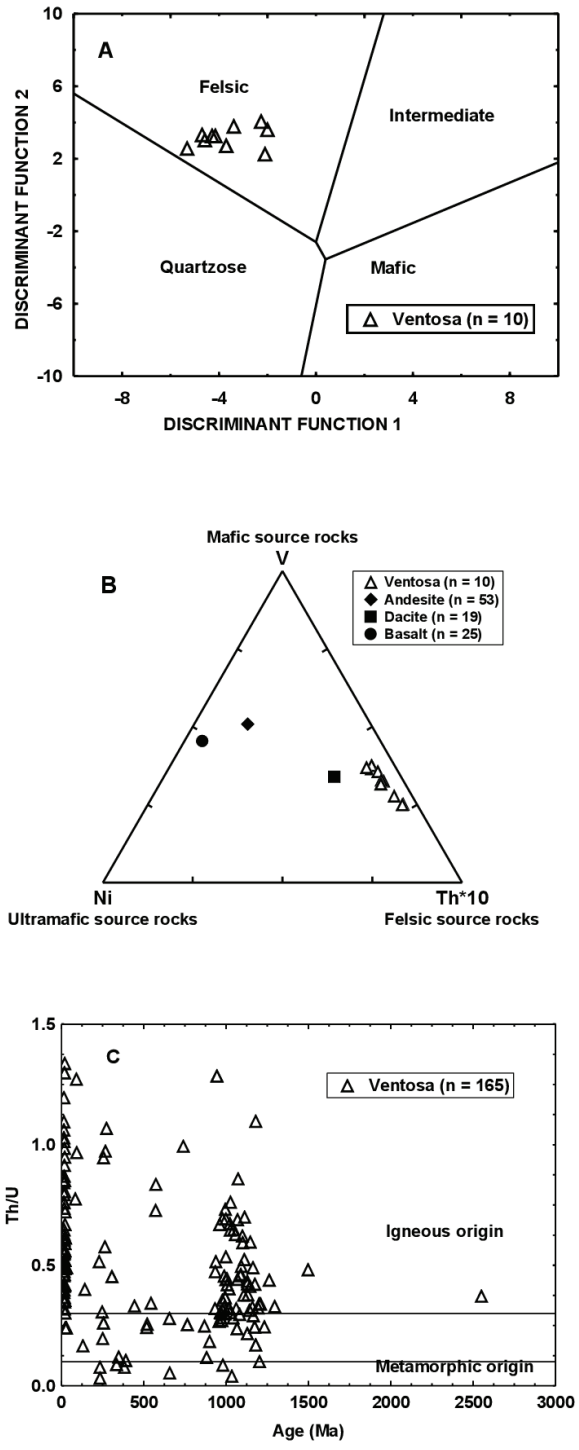

Fig. 8. (A) Major element based discriminant function diagram to infer sediment provenance (Roser & Korsch 1988). The discriminant functions are: Discriminant Function 1=(−1.773*TiO_2)+(0.607*Al_2O_3)+(0.760*Fe_2O_3)+(−1.500*MgO)+(0.616*CaO)+(0.509*Na_2O)+(−1.224*K_2O)+(−9.090); Discriminant Function 2=(0.445*TiO_2)+(0.070*Al_2O_3)+(−0.250*Fe_2O_3)+(−1.142*MgO)+(0.438*CaO)+(1.475*Na_2O)+(1.426*K_2O)+(−6.861). **(B)** Ni–Th*10–V ternary diagram (Bracciali et al. 2007) for the Ventosa beach sediments. Average compositions of dacite, andesite, and basalt are also plotted for comparison (Condie 1993). **(C)** Bivariate plot of Th/U versus U–Pb ages of detrital zircon grains from the Ventosa beach sediments, Mexican Pacific.

from other formations, i.e. Todos Santos Formation in the southern Isthmus of Tehuantepec. These authors reported Mesoproterozoic age with intervals between ~ 1002 Ma and 1503 Ma. Similarly, the Río Hondo Formation from the same region reveal ages from ~ 1013 Ma to 1255 Ma.

Considering the second age group Cenozoic, among 64 concordant single-grain ages, 43.8 % of which form a youngest peak of 22 Ma. The U–Pb ages range between 18 Ma and 24 Ma, which are comparable to the Basal Ixtapa Formation (~19–22 Ma). A white tuffaceous/ash layer from the Río Hondo unit of the Ixtapa Formation indicates an age of ~12 Ma. In addition, based on the $^{40}Ar/^{39}Ar$ method, Camprubí et al. (2019) dated the geochronological ages of the Zacatepec mineral deposits near the Tehuantepec coastal area, which yielded an isochron age of 17±0.4 Ma for hornblende (13±0.5 Ma–21±0.9 Ma) and 18±0.1 Ma for biotite (14±4 Ma–18±0.3 Ma), both corresponds to an Early Miocene age. Also, Pindell et al. (2020) reported Miocene age for the magmatic rocks at the southwestern Isthmus of Tehuantepec region (~11.2–22.8 Ma; Fig. 10). The similarities in U–Pb ages between this study and source terranes in the Isthmus of Tehuantepec region, i.e. Todos Santos, Ixtapa, and Huamelula Formations are illustrated in Fig. 11.

Furthermore, in the Oaxaca State, there are Cenozoic plutons, which extend discontinuously for approximately 380 km with ages varying between 15 and 56 Ma. These Cenozoic plutons reveal Eocene–Miocene tectono-magmatic evolution of the continental margin of Oaxaca (Morán-Zenteno et al. 2022). Also, dating of zircon grains from the Cuicateco terrane, Oaxaca State (volcano sedimentary sequence) indicates younger ages varying from ~1.2 Ma to 65.7 Ma, which consists of conglomerates with clasts of granite and andesite (Ángeles-Moreno 2006). The circulation in the Gulf of Tehuantepec influences the transport of sediments from Chiapas to the Oaxaca coast, this predominately composed of tidal (towards northwestern direction) and wind-driven "Tehuanos" currents.

Statistical analysis

F-test with 95 % confidence is calculated to analyze the zircon grains age variation, which compares the F statistic to a quantile of the F distribution. The results are listed in Table 9, which suggest that two samples have statistically different variances, also their distribution is different. It can be inferred that sample V1 is more influenced by the contribution of sediments from the distant source area, while V2 has a greater influence by the nearby source areas within the Oaxaca State dominated by Miocene ages.

Conclusions

The mineralogy, geochemistry, and zircon grains U–Pb ages in the Ventosa beach sediments provide the following conclusions:

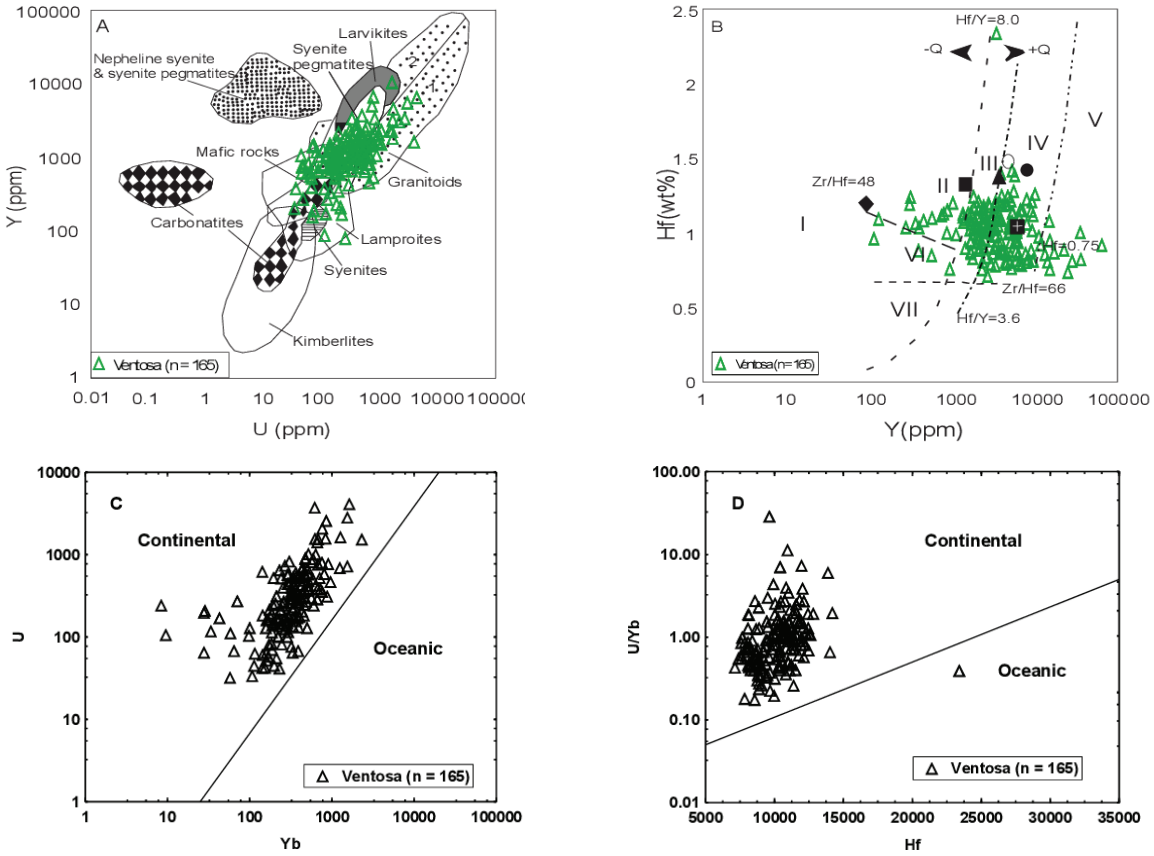

Fig. 9. Bivariate plots for the zircon grains recovered in the Ventosa beach, Mexican Pacific. **(A)** Y versus U (fields are after Belousova et al. 2002); **(B)** Hf versus Y (fields are after Shnukov et al. 1989); **(C)** U versus Yb (after Grimes et al. 2007) and **(D)** U/Yb versus Hf (after Grimes et al. 2007). I=kimberlites, II=ultramafic, mafic and intermediate rocks, III=quartz-bearing intermediate and felsic rocks, IV=felsic rocks with high SiO_2 content, V=greisens, VI=alkaline rocks and alkaline metasomatites of alkaline complexes, and VII=carbonatites.

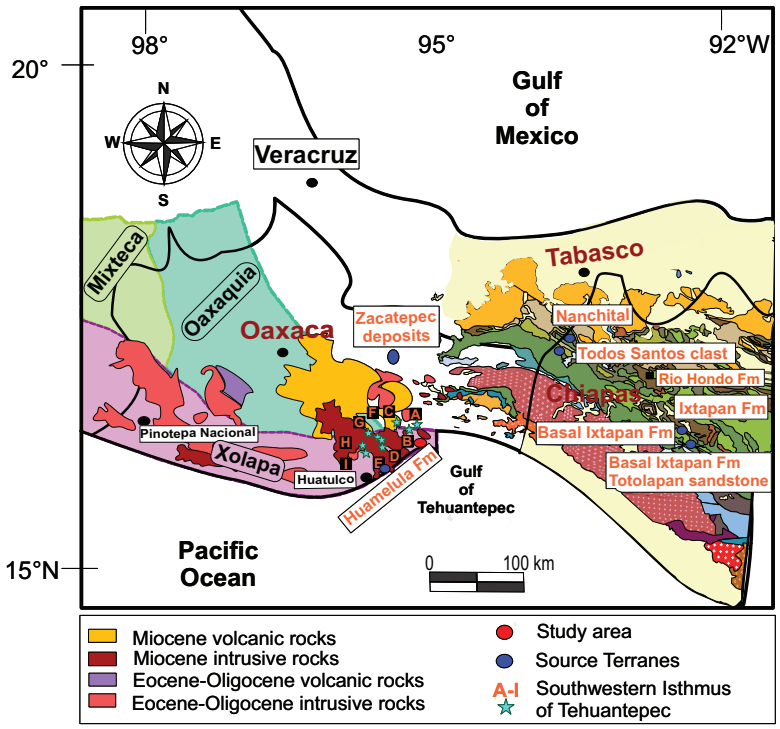

Fig. 10. Map showing possible source terranes for the Ventosa beach sediments. The terranes compared from the southwestern coast of Oaxaca are: Nanchital, Todos Santos clast, Huamelula Formation, Basal Ixtapan Formation, Totolapan sandstone, zircon grains dated from hornblende and biotites (Zacatepec deposits), and zircon grains dated from the southwestern Isthmus of Tehuantepec (A–I) (Camprubí et al. 2019; Molina-Garza et al. 2020; Pindell et al. 2020, 2023). Map modified after the Dirección General de Geografía del Territorio Nacional, 2025, Scale 1:1,000,000. Fm=Formation.

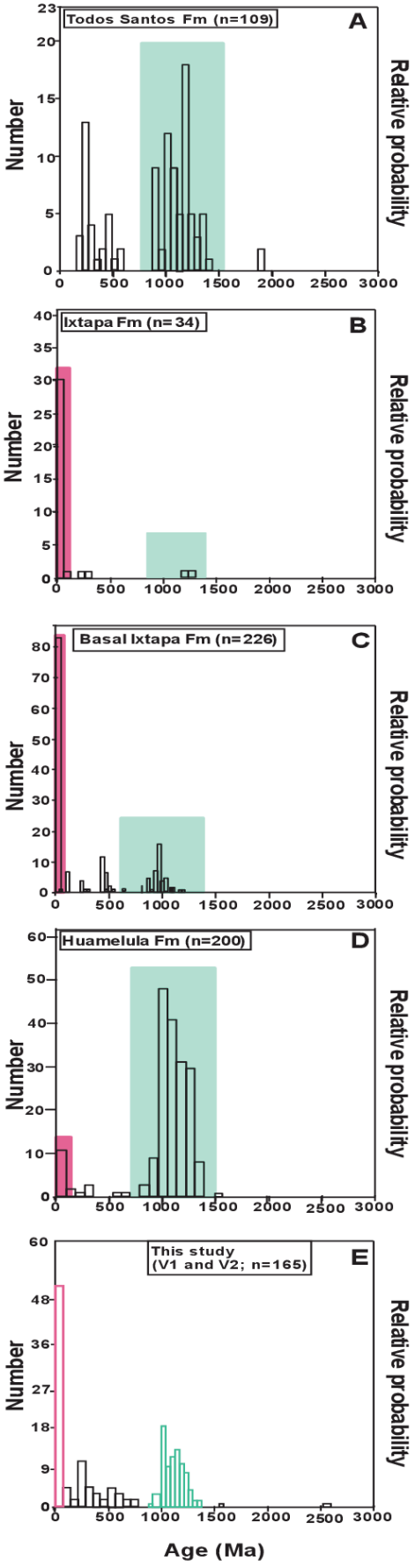

Fig. 11. Histograms for age comparison between potential source terranes and this study. **(A)** Todos Santos Formation; **(B)** Ixtapa Formation; **(C)** Basal Ixtapa Formation; **(D)** Huamelula Formation; **(E)** This study; Fm=Formation. Pink and green color shades indicate the predominant age similarities between this study and potential source terranes. Age distribution data of zircon grains from the potential source terranes are from Camprubí et al. (2019) and Pindell et al. (2020, 2023). The locations of source terranes are shown in Fig. 9.

Table 9: F test for samples V1 and V2.

	V2	*V1*
Median	289.80	734.95
Variance	192383.26	238456.04
Observations	65	100
Degrees of freedom	64	99
F	0.80	
P(F<=f) a queue	0.17	
Critical value for F (a queue)	0.68	

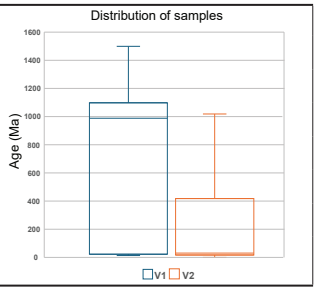

- The dominant minerals in sediments are quartz, K-feldspar, anorthite, zircon, and magnetite. The CIA, PIA, and CIW values indicate moderate chemical weathering in the source area. The chemical composition of bulk sediments suggests that they were derived from the felsic igneous rocks such as granite and granitoids, which is also consistent with the Qt_{68}–Ft_{6}–Lt_{26} modal components. The REE patterns are homogeneous with a little negative Eu anomaly, which is also a characteristic of felsic igneous rocks. The environmental indices like EF, I_{geo}, PLI, and RI indicate an anthropogenic source for the element Cu, simultaneously is a risk to the aquatic environment and health.
- The U–Pb ages of zircon grains show the abundance of Cenozoic (~ 12.9 – 31.2 Ma) and Proterozoic ages (~ 657–1499 Ma). Based on the U–Pb ages, we inferred that the sediments were supplied from the nearby Todos Santos, Ixtapa, and Huamelula Formations, and were distributed in the Gulf of Tehuantepec by fluvial and littoral currents. Although the beach sediments were derived from a mixed origin, the sediment composition and geochronology of zircon grains of this study show high similarity with the nearby terranes.

Acknowledgements: Ramos-Vázquez is grateful to the SECIHTI for the postdoctoral fellowship (CVU: 595593). Armstrong-Altrin is thankful to the PAPIIT (IN104824) and Institutional (ICML-616) projects. We are grateful to Carlos L. López, Laura E. Gómez Lizárraga, Arturo R. Arvizu, and Teodoro H. Treviño, for the analytical help. Dr. Luigi Solari, Irene Pérez, and Carlos Ortega-Obregón for zircon grains dating. We appreciate Barbara Perez for her participation during sample collection at the Ventosa Beach. We are grateful to the reviewers A. Vozárová and E. Juárez-Arriaga, and the Associate Editor for their comments, which improved our presentation.

References

Andersen T., Elburg M.A. & Magwaza B.N. 2019: Sources of bias in detrital zircon geochronology: Discordance, concealed lead loss and common lead correction. *Earth-Science Reviews* 197, 102899. https://doi.org/10.1016/j.earscirev.2019.102899

Andreasen N., Jackson R., Rudra A., Nøhr-Hansen H., Sanei H., Bojesen-Koefoed J., Seidenkrantz M.S., Pearce C., Thibault N. & Ribeiro S. 2023: From land to sea: provenance, composition, and preservation of organic matter in a marine sediment record from the North-East Greenland shelf spanning the Younger Dryas–Holocene. *Boreas* 52, 459–475. https://doi.org/10.1111/bor.12630

Ángeles-Moreno E. 2006: Petrografía, geología estructural y geocronología del borde noroccidental del terreno Cuicateco, Sierra Mazateca, Estado de Oaxaca, México. *MSc thesis. Universidad Nacional Autónoma de México*, Mexico City.

Aranda-Gómez J.J., Juárez-Arriaga E., Chávez-Cabello G., Ramírez-Peña C.F., Treviño-Rodríguez F., Yutsis V., Samuel Eguiluz y de Antuñano & González M.V. 2024: Structural architecture of the Mapimí Biosphere Reserve and its surroundings, north-central Mexico: New insights from U–Pb geochronology and interpreted structural data. *Journal of South American Earth Sciences* 141, 104924. https://doi.org/10.1016/j.jsames.2024.104924

Armstrong-Altrin J.S. 2020: Detrital zircon U–Pb geochronology and geochemistry of the Riachuelos and Palma Sola beach sediments, Veracruz State, Gulf of Mexico: a new insight on palaeoenvironment. *Journal of Palaeogeography* 9, 28. https://doi.org/10.1186/s42501-020-00075-9

Armstrong-Altrin J.S. 2024: U–Pb ages of zircon grains in the Playa Azul Beach Sediments, Guerrero State, Mexican Pacific. *Journal of the Geological Society of India* 100, 1373–1384. https://doi.org/10.17491/jgsi/2024/173993

Armstrong-Altrin J.S., Ramos-Vázquez M.A., Zavala-León A.C. & Montiel-García P.C. 2018: Provenance discrimination between Atasta and Alvarado beach sands, western Gulf of Mexico, Mexico: Constraints from detrital zircon chemistry and U–Pb geochronology. *Geological Journal* 53, 2824–2848. https://doi:org/10.1002/gj.3122

Armstrong-Altrin J.S., Ramos-Vázquez M.A., Hermenegildo-Ruiz N.Y. & Madhavaraju J. 2021: Microtexture and U–Pb geochronology of detrital zircon grains in the Chachalacas beach, Veracruz State, Gulf of Mexico. *Geological Journal* 56, 2418–2438. https://doi.org/10.1002/gj.3984

Ayala-Pérez M.P., Armstrong-Altrin J.S. & Machain-Castillo M.L. 2021: Heavy metal contamination and provenance of sediments recovered at the Grijalva River delta, southern Gulf of Mexico. *Journal of Earth System Science* 130. https://doi.org/10.1007/s12040-021-01570-w

Azamar Alonso A. & Tellez Ramírez I. 2021: Efectos multidimensionales de la minería en San José del Progreso, Oaxaca. *Región y Sociedad* 33, e1471.

Bahr F. & Keighley D. 2021: Chemostratigraphy of Cumberland Group (Pennsylvanian) strata influenced by salt tectonics, Joggins Fossil Cliffs UNESCO World Heritage Site, eastern Canada. *Journal of Sedimentary Research* 91, 969–985. https://doi.org/10.2110/jsr.2020.152

Belousova E.A., Griffin W.L., O'Reilly S.Y. & Fisher N.I. 2002: Igneous zircon: trace element composition as an indicator of source rock type. *Contributions to Mineralogy and Petrology* 143, 602–622. https://doi.org/10.1007/s00410-002-0364-7

Bónová K., Bóna J., Gallay M., Hók J., Bella P., Pańczyk M., Hraško L. & Mikuš T. 2024: Reconstruction of ancient drainage in the contact karst of the Harmanecká dolina Valley, Western Carpathians, based on mineralogical data from the allochthonous sediments and isobase geomorphometry. *Earth Surface Processes and Landforms* 49, 1682–1704. https://doi.org/10.1002/esp.5780

Botello A.V., Villanueva S.F., Díaz G. & Escobar-Briones E. 1998: Polycyclic aromatic hydrocarbons in sediments from Salina Cruz Harbor and coastal areas, Oaxaca, Mexico. *Marine Pollution Bulletin* 36, 554–558. https://doi.org/10.1016/S0025-326X(98)00026-5

Bracciali L., Marroni M., Luca P. & Sergio R. 2007: Geochemistry and petrography of Western Tethys Cretaceous sedimentary covers (Corsica and Northern Apennines): From source areas to configuration of margins. In: Arribas J., Johnsson M.J. & Critelli S. (Eds.): Sedimentary Provenance and Petrogenesis: Perspectives from Petrography and Geochemistry. *Geological Society of America*. https://doi.org/10.1130/2006.2420(06)

Camprubí A., Cabrera-Roa M.A., González-Partida E. & López-Martínez M. 2019: Geochronology of Mexican mineral deposits. VIII: the Zacatepec polymetallic skarn, Oaxaca. *Boletín de la Sociedad Geológica Mexicana* 71, 207–218. https://doi.org/10.18268/bsgm2019v71n1a11

Castillo-Nieto F., Rodriguez-Luna E., Castro-Mora J., Arceo y Carilla F., Carranza-Alvarado M., Gómez-Caballero J.A., Pérez-León C., Hernandez-Hernández J., Rivas-Ayala M.A. & Enriquez-Borja V.M. 1996: Monografía Geológico-Minera del Estado de Oaxaca. *Consejo de Recursos Minerales*, 1–280.

Chen Y., Li J., Chen L., Zhang B. & Zhao H. 2025: Early Cretaceous tuffs from the southwestern Ordos Basin, North China Craton: Geochronology, geochemistry and geological significance. *Geological Journal* 60, 1559–1575. https://doi.org/10.1002/gj.5143

Chougong D.T., Bessa A.Z.E., Ngueutchoua G., Yongue R.F., Ntyam S.C. & Armstrong-Altrin J.S. 2021: Mineralogy and geochemistry of Lobé River sediments, SW Cameroon: Implications for provenance and weathering. *Journal of African Earth Sciences* 183, 104320. https://doi.org/10.1016/j.jafrearsci.2021.104320

Christophoridis C., Dedepsidis D. & Fytianos K. 2009: Occurrence and distribution of selected heavy metals in the surface sediments of Thermaikos Gulf, N. Greece. Assessment using pollution indicators. *Journal of Hazardous Materials* 168, 1082–1091. https://doi.org/10.1016/j.jhazmat.2009.02.154

CONAGUA (Comisión Nacional del Agua) 2002: Estudio de actualización de mediciones piezométricas en los acuíferos Tehuantepec, Río Ostuta, Nochixtlán y Huatulco del estado de Oaxaca, y Cuajinicuilapa del estado de Guerrero. Realizado por COPEI, Ingeniería, S.A. de C.V.

Condie K.C. 1993: Chemical composition and evolution of the upper continental crust: contrasting results from surface samples and shales. *Chemical Geology* 104, 1–37. https://doi.org/10.1016/0009-2541(93)90140-E

Cox R., Lowe D.R. & Cullers R.L. 1995: The influence of sediment recycling and basement composition on evolution of mudrock chemistry in the southwestern United States. *Geochimica et Cosmochimica Acta* 59, 2919–2940. https://doi.org/10.1016/0016-7037(95)00185-9

CRM (Consejo de Recursos Minerales) 1996: Monografía Geológico–Minera del Estado de Oaxaca. México City, Mexico.

De Falco G., Molinaroli E., Baroli M. & Bellacicco S. 2003: Grain size and compositional trends of sediments from Posidonia Oceanica meadows to beach shore, Sardinia, western Mediterranean. *Estuarine, Coastal and Shelf Science* 58, 299–309. https://doi.org/10.1016/S0272-7714(03)00082-9

Dickinson W.R. 1970: Interpreting detrital modes of greywacke and arkose. *Journal of Sedimentary Petrology* 40, 695–707.

Dickinson W.R. 1985: Interpreting provenance relation from detrital modes of sandstones. In: Zuffa G.G. (Ed.): Provenance of Arenites: NATO ASI Series, C 148. *D. Reidel Publishing Company*, Dordrecht, 333–363.

Djibril K.N.G., Yiika L.P., Etutu M.E.M.M., Eric B.E., Mengu E.E., Jean-Lavenir N.M. & Armstrong-Altrin J.S. 2024: Geochemistry of sediments from the Mugheb River, Bamenda, Cameroon volcanic line: implications for provenance, paleoweathering and tectonic setting. *Arabian Journal of Geosciences* 17, 331. https://doi.org/10.1007/s12517-024-12148-3

dos Santos R.F., Figueira R.C.L., Burone L., de Rezende C.E. & de Mahiques M.M. 2025: Tracing geochemical footprints in surface sediments of the southwest Atlantic margin: a journey through the Santos, Campos, Pelotas, and Punta del Este Basins. *Geo-Marine Letters* 45, 10. https://doi.org/10.1007/s00367-025-00798-5

Elbakhouch N., Ahmed T., Armstrong-Altrin J.S., Hassan I. & Driss C. 2025: Geochemical composition of the Ediacaran and Cambrian shales from the Tighardine region, Western High-Atlas, Morocco: implications for depositional environments, paleoclimate, and paleoweathering. *Journal of African Earth Sciences* 234, 105933. https://doi.org/10.1016/j.jafrearsci.2025.105933

Elizondo-Pacheco L.A., Solari L.A., He H.L., Ramírez-Fernández J.A. & Maldonado R. 2025: Revisiting Oaxaquia-Laurentia connections during Rodinia assembly: Insights from u-pb dating and geochemistry of massif-type anorthosite intrusions and associated rocks from the northern Oaxacan Complex, southern Mexico. *Precambrian Research* 420, 107726. https://doi.org/10.1016/j.precamres.2025.107726

Farmer G.L. 2003: Continental basaltic rocks. In: Rudnick R.L. (Ed): *Treatise on Geochemistry* 3, 85–122. https://doi.org/10.1016/B0-08-043751-6/03019-X

Fedo C.M., Nesbitt W.H. & Young G.M. 1995: Unraveling the effects of potassium metasomatism in sedimentary rocks and paleosols, with implications for paleoweathering conditions and provenance. *Geology* 23, 921–924. https://doi.org/10.1130/0091-7613

Felicio dos Santos R., Figueira R.C.L., Burone L., Eduardo de Rezende C. & Michaelovitch de Mahiques M. 2025: Tracing geochemical footprints in surface sediments of the southwest Atlantic margin: a journey through the Santos, Campos, Pelotas, and Punta del Este Basins. *Geo-Marine Letters* 45, 10. https://doi.org/10.1007/s00367-025-00798-5

Fiedler P.C. & Lavín M.F. 2017: Oceanographic conditions of the eastern tropical pacific. In: Glynn P.W., Manzello D.P. & Enochs I.C. (Eds.): Coral Reefs of the Eastern Tropical Pacific. Coral Reefs of the World 8. *Springer*, Dordrecht, 59–83. https://doi.org/10.1007/978-94-017-7499-4_3

Flores-Castro M. & Armstrong-Altrin J.S. 2022: Textural characteristics and abundance of microplastics in Tecolutla beach sediments, Gulf of Mexico. *Environmental Monitoring and Assessment* 194, 752. https://doi.org/10.1007/s10661-022-10447-4

Flores-Ocampo I.Z., Armstrong-Altrin J.S., Fernández-Guevara G.D., Madhavaraju J., Acevedo-Granados I.V., Pérez-Alvarado B.Y., Ibarra-Rueda S.E., Flores-Cortés M. & Guadalupe-Díaz I. 2025: Geochemical and geochronological constraints on the provenance and heavy metal contamination of beach sediments along the Gulf of Mexico, Mexico. *Minerals* 15, 1277. https://doi.org/10.3390/min15121277

Gehrels G. 2014: Detrital Zircon U–Pb Geochronology Applied to Tectonics. *Annual Review of Earth and Planetary Sciences* 42, 127–149. https://doi.org/10.1146/annurev-earth-050212-124012

Girão A.V., Caputo G. & Ferro M.C. 2017: Application of Scanning Electron Microscopy-Energy Dispersive X-Ray Spectroscopy (SEM-EDS). *Comprehensive Analytical Chemistry* 75, 153–168. https://doi.org/10.1016/bs.coac.2016.10.002

Grimes C.B., John B.E., Kelemen P.B., Mazdab F.K., Wooden J.L., Cheadle M.J., Hanghøj K. & Schwartz J.J. 2007: Trace element chemistry of zircons from oceanic crust: a method for distinguishing detrital zircon provenance. *Geology* 35, 643–646. https://doi.org/10.1130/G23603A.1

Håkanson L. 1980: An ecological risk index for aquatic pollution control. A sedimentological approach. *Water Research* 14, 975–1001. https://doi.org/10.1016/0043-1354(80)90143-8

Harnois L. 1988: The CIW index: A new chemical index of weathering. *Sedimentary Geology* 55, 319–322. https://doi.org/10.1016/0037-0738(88)90137-6

Hendy I.L. & Pedersen T.F. 2006: Oxygen minimum zone expansion in the eastern tropical North Pacific during deglaciation. *Geophysical Research Letters* 33, L20602. https://doi.org/10.1029/2006GL025975

Hermann J. & Rubato D. 2009: Accessory phase control on the trace element signature of sediment melts in subduction zones. *Chemical Geology* 265, 512–526. https://doi.org/10.1016/j.chemgeo.2009.05.018

Hossain H.M.Z., Al Hossain A., Islam Md. A., Liu Z. & Yu M 2025: Geochemistry of Core Sediments from the Southeast Coast of Bangladesh: Constraints on Chemical Weathering, Paleoenvironmental Conditions, Provenance, and Tectonic Setting. *Geological Journal* 60, 1252–1269. https://doi.org/10.1002/gj.5122

Imai N., Terashima S., Itoh S. & Ando A. 1995: 1994 compilation values for GSJ reference samples, "Igneous rock series". *Geochemical Journal* 29, 91–95. https://doi.org/10.2343/geochemj.29.91

Ingersoll R.V., Bulard T.F., Ford R.L., Grimn J.P., Pickle J.P. & Sares S.W. 1984: The effect of grain size on detrital modes: a test of the Gazzi-Dickinson point counting method. *Journal of Sedimentary Petrology* 54, 103–116. https://doi.org/10.1306/212F83B9-2B24-11D7-8648000102C1865D

INEGI (Instituto Nacional de Estadística y Geografía) 2008: Anuario estadístico. *Veracruz de Ignacio de Llave Tomo* 1, 605.

Islam A.R.M.T., Rabbi A.H.M.F., Anik A.H., Khan R., Masud M.A.A., Nedjoud G., Idris A.M., Rahman M.N. & Senapathi V. 2025: Source distribution, ecological risks, and controlling factors of heavy metals in river sediments: Receptor model-based study in a transboundary river basin. *International Journal of Sediment Research* 1, 45–61. https://doi.org/10.1016/j.ijsrc.2024.10.001

Janpou A.K., Ekoa Bessa A.Z., Ntouala D.R.F., Kelepile T., Ngueutchoua G. & Armstrong-Altrin J.S. 2024: Provenance of beach sands in the northern Gulf of Guinea, SW Cameroon. *Journal of the Geological Society of India* 100, 99–114. https://doi.org/10.17491/jgsi/2024/172987

Kanwel S., Gulzar F., Alofaysan H., Tanriverdiyev S. & Jing H. 2025: Toxic metal pollution in freshwater ecosystems: A systematic review of assessment methods using environmental and statistical indices. *Marine Pollution Bulletin* 218, 118028. https://doi.org/10.1016/j.marpolbul.2025.118028

Kasanzu C.H. 2025: Geochemical characterization of the Cenomanian–Campanian Red Sandstone Group of the Rukwa Basin, SW Tanzania: implications for provenance, paleoclimate and paleo-redox conditions. *Journal of Sedimentary Environments* 10, 635–668. https://doi.org/10.1007/s43217-025-00231

Leikin S. & Phillips A. 2023: ICP-OES as a viable alternative to ICP-MS for trace analysis: Meeting the detection limits challenge. *Spectroscopy* 38, 7–13. https://doi.org/10.56530/spectroscopy.do3475y9

Lozano R. & Bernal J.P. 2005: Characterization of a new set of eight geochemical reference materials for XRF, major and trace element analysis. *Revista Mexicana de Ciencias Geológicas* 22, 329–344. https://www.rmcg.unam.mx/index.php/rmcg/article/view/ 841

Ludwig K.R. 2003: User's Manual for Isoplot 3.00: A Geochronological Toolkit for Microsoft Excel. *Special Publication 4a, Berkeley Geochronological Centre*, Berkeley, California.

Madhavaraju J., Noriega-Montoya D.G., Ramirez-Montoya E., González-León C.M. & Armstrong-Altrin J.S. 2024: Provenance and tectonic setting of sandstones of Lomas Coloradas Formation, Cabullona Group, Sonora, Mexico: Constraints on petrography and geochemistry. *Journal of Palaeogeography* 13, 839–861. https://doi.org/10.1016/j.jop.2024.07.005

Molina-Garza R.S., Lawton T.F., Barboza Gudiño J.R., Sierra-Rojas M.I., Figueroa Guadarrama A. & Pindell J. 2020: Geochronology and correlation of the Todos Santos Group, western Veracruz and

eastern Oaxaca States, Mexico: Implications for regional stratigraphic relations and the rift history of the Gulf of Mexico. In: Martens U. & Molina Garza R.S. (Eds.): Southern and Central Mexico: Basement Framework, Tectonic Evolution, and Provenance of Mesozoic–Cenozoic Basins. *The Geological Society of America Special Papers* 546. https://doi.org/10.1130/2020.2546(06)

Moore S., Heise E.A., Grove M., Reisinger A. & Benavides J.A. 2021: Evaluating the impacts of dam construction and longshore transport upon modern sedimentation within the Rio Grande Delta (Texas, U.S.A.). *Journal of Coastal Research* 37, 26–40. https://doi.org/10.2112/JCOASTRES-D-20-00049.1

Morán-Zenteno D., Martiny B., Solari L., Mori L., Luna-González L. & González-Torres E. 2018: Cenozoic magmatism of the Sierra Madre del Sur and tectonic truncation of the Pacific margin of southern Mexico. *Earth Science Reviews* 183, 85–114. https://doi.org/10.1016/j.earscirev.2017.01.010

Morán-Zenteno D.J., Martiny B.M., García-Rodríguez H.M., García-Hernández S.Y., Ortiz-Olvera V., Muñoz-Rojas E.R., Solari L. & Ortega-Obregón C. 2022: U–Pb geochronology of Cenozoic plutons in the Pinotepa Nacional–Salina Cruz region and patterns in the migration of magmatism along the SW continental margin of Mexico. *International Journal of Earth Sciences (Geol Rundsch)* 111, 717–746. https://doi.org/10.1007/s00531-021-02145-2

Müller G. 1969: Index of geoaccumulation in sediments of the Rhine River. *GeoJournal* 2, 108–118.

Ndjigui P.D., Beauvais A., Fadil-Djenabou S. & Ambrosi J.P. 2014: Origin and evolution of Ngaye river alluvial sediments, Northern Cameroon: Geochemical constraints. *Journal of African Earth Sciences* 100, 164–178. https://doi.org/10.1016/j.jafrearsci.2014.06.005

Nesbitt H.W. & Young G.M. 1982: Prediction of Some Weathering Trends of Plutonic and Volcanic Rocks Based on Thermodynamic and Kinetic Considerations. *Geochimica et Cosmochimica Acta* 48, 1523–1534. https://doi.org/10.1016/0016-7037(84)90408-3

Ortega-Gutiérrez F., Elías-Herrera M., Morán-Zenteno D.J., Solari L., Weber B. & Luna-González L. 2018: The pre-Mesozoic metamorphic basement of Mexico, 1.5 billion years of crustal evolution. *Earth Science Reviews* 183, 2–37. https://doi.org/10.1016/j.earscirev.2018.03.006

Pauli de Castro A., Ferreira Guedes C.C., Farias Vesely F., Marli da Silveira D. & Ferreira Neves L. 2023: Provenance, diagenesis and reservoir quality of sandstone facies of the Maracangalha Formation, Recôncavo Basin – Northeastern Brazil. *Marine and Petroleum Geology* 158, Part B 106548.

Pérez-Alvarado B.Y. & Armstrong-Altrin J.S. 2025: Microplastics in the Barra Norte and Mocambo beach sediments, Gulf of Mexico, Mexico. *Carpathian Journal of Earth and Environmental Sciences* 20, 241–254. https://doi.org/10.26471/cjees/2025/020/329

Pindell J., Molina-Garza R., Villagómez D., Martens U., Graham R., Stockli D., Weber B. & Sierra-Rojas M.I. 2020: Provenance of the Miocene Nanchital conglomerate, western Chiapas Fold belt, Mexico: implications for reservoir sands in the Sureste Basin, Greater Campeche Province. *Geological Society, London, Special Publications* 504, 167–182. https://doi.org/10.1144/SP504-2020-12

Pindell J., Villagomez D., Garza R.M., Beltran A., Stockli D.F. & Wildman M. 2023: Late Cretaceous–Miocene depositional evolution of Chiapas, Mexico: A foreland controlled by collision of Greater Antilles arc and the subsequent relative migration of the Chortís block. *Gondwana Research* 113, 116–143. https://doi.org/10.1016/j.gr.2022.10.016

Ramos-Vázquez M.A. 2021: Procedencia de sedimentos detríticos de playas y mar profundo del Golfo de México, Mexico City. *Ph.D thesis, Universidad Nacional Autónoma de México*, 1–253. https://repositorio.unam.mx/contenidos/3584669

Ramos-Vázquez M.A. 2023: Sediment provenance inferred by U–Pb ages of zircon grains in the Puerto Chiapas beach, Mexican Pacific. *Arabian Journal of Geosciences* 16, 266. https://doi.org/10.1007/s12517-023-11363-8

Ramos-Vázquez M.A. & Armstrong-Altrin J.S. 2019: Sediment chemistry and detrital zircon record in the Bosque and Paseo del Mar coastal areas from the southwestern Gulf of Mexico. *Marine and Petroleum Geology* 110, 650–675. https://doi.org/10.1016/j.marpetgeo.2019.07.032

Ramos-Vázquez M.A. & Armstrong-Altrin J.S. 2021: Provenance of sediments from Barra del Tordo and Tesoro beaches, Tamaulipas State, northwestern Gulf of Mexico. *Journal of Palaeogeography* 10, 20. https://doi.org/10.1186/s42501-021-00101-4

Ramos-Vázquez M.A., Armstrong-Altrin J.S., Machain-Castillo M.L. & Gío-Argáez F.R. 2018: Foraminiferal assemblages, ^{14}C ages, and compositional variations in two sediment cores in the western Gulf of Mexico. *Journal of South American Earth Sciences* 88, 480–496. https://doi.org/10.1016/j.jsames.2018.08.025

Ramos-Vázquez M.A., Verma S.K., Armstrong-Altrin J.S., Arthur James R. & Madhavaraju J. 2024a: Characterization of microplastics in marine sediments from the Gulf of Tehuantepec, Mexican Pacific. *Carpathian Journal of Earth and Environmental Sciences* 19, 255–264. https://doi.org/10.26471/cjees/2024/019/296

Ramos-Vázquez M.A., Armstrong-Altrin J.S., Fernández-Guevara G.D., Madhavaraju J., Verma S.K. & James R.A. 2024b: Provenance of sediments and environmental risk assessment of heavy metals in the "Mis Amores" beach, Veracruz, Gulf of Mexico, Mexico. *Journal of the Indian Association of Sedimentologists* 41, 55–67. https://doi.org/10.51710/jias.v41iI.355

Roser B.P. & Korsch R.J. 1988: Provenance signatures of sandstone-mudstone suites determined using discriminant function analysis of major-element data. *Chemical Geology* 67, 119–139. https://doi.org/10.1016/0009-2541(88)90010-1

Rudnick R.L. & Gao S. 2003: Composition of the continental crust. In: Rudnick R.L. (Ed.): The crust 3. *Treatise on Geochemistry,* 1–64. https://doi.org/10.1016/B0-08-043751-6/03016-4

Sai Babu S., Rao V.P. & Mohan M.R. 2024: Controls on the distribution and fractionation of rare earth elements in recent sediments from the rivers along the west coast of India. *Environmental Earth Sciences* 83, 547. https//doi.org/10.21203/rs.3.rs-4452724/v1

SGM (Servicio Geológico Mexicano) 2021: Panorama Minero del Estado de Oaxaca. *Dirección de Investigación y Desarrollo,* 1–49.

Sharman G.R., Covault J.A., Stockli D.F., Sickmann Z.T., Malkowski M.A. & Johnstone S.A. 2021: Detrital signals of coastal erosion and fluvial sediment supply during glacio-eustatic sea-level rise, Southern California, USA. *Geology* 49, 1501–1505. https://doi.org/10.1130/G49430.1

Shnukov S.E., Cheburkin A.K. & Andreev A.V. 1989: Geochemistry of wide-spread coexisting accessory minerals and their role in investigation of endogenic and exogenic processes. *Geological Journal* 2, 107–114.

Shukla M., Verma S.K., Ramos-Vázquez M.A., Armstrong-Altrin J.S., Mishra S., Oliveira E.P. & González-Partida E. 2024: Geochemistry and U–Pb geochronology of detrital zircon grains in beach sediments from the northwestern Gulf of Mexico, Tamaulipas, Mexico: Implication for provenance. *Applied Geochemistry* 174, 106148. https://doi.org/10.1016/j.apgeochem.2024.106148

Shukla M., Verma S.K., Armstrong-Altrin J.S., Ramos-Vázquez M.A., Mishra S., Oliveira E.P., González-Partida E., Hernández-Mendoza H. & Malviya V.P. 2025: Identification of source terranes of beach sediments from the NW Gulf of Mexico, Atlantic Ocean: Constraints from geochemistry and U–Pb detrital zircon geo-

chronology. *Journal of South American Earth Sciences* 158, 105496. https://doi.org/10.1016/j.jsames.2025.105496

Sláma J., Košler J., Condon D.J., Crowley J.L., Gerdes A., Hanchar J.M., Horstwood M.S.A., Morris G.A., Nasdala L., Norberg N., Schaltegger U., Schoene B., Tubrett M.N. & Whitehouse M.J. 2008: Plešovice zircon – A new natural reference material for U–Pb and Hf isotopic microanalysis. *Chemical Geology* 249, 1–35. https://doi.org/10.1016/j.chemgeo.2007.11.005

Sopie F.T., Ngueutchoua G., Armstrong-Altrin J.S., Njanko T., Sonfack A.N., Ngagoum Y.S.K., Fossa D. & Tembu L.T. 2023: Provenance, weathering, and tectonic setting of the Yoyo, Kribi, and Campo beach sediments in the southern Gulf of Guinea, SW Cameroon. *Journal of Earth System Science* 132, 92. https://doi.org/10.1007/s12040-023-02101-5

Suttner L.J. & Basu A. 1985: The effect of grain size on detrital modes: a test of the Gazzi- Dickinson point-counting method. *Journal of Sedimentary Petrology* 55, 616–617.

Tapia-Fernández H.J., Armstrong-Altrin J.S. & Selvaraj K. 2017: Geochemistry and U-Pb geochronology of detrital zircons in the Brujas beach sands, Campeche, Southwestern Gulf of Mexico, Mexico. *Journal of South American Earth Sciences* 76, 346–361. https://doi.org/10.1016/j.jsames.2017.04.003

Tawfik H.A., Salah M.K., Maejima W., Armstrong-Altrin J.S., Abdel-Hameed A-M.T. & Ghandour M.M.E. 2018: Petrography and geochemistry of the Lower Miocene Moghra sandstones, Qattara Depression, north Western Desert, Egypt. *Geological Journal* 53, 1938–1953. https://doi.org/10.1002/gj.3025

Taylor S.R. & McLennan S.M. 1985: The Continental Crust: its Composition and Evolution. *Blackwell*, Malden, MA, 312.

Tomlinson D.L., Wilson J.G., Harris C.R. & Jeffrey D.W. 1980: Problems in the assessment of heavy-metal levels in estuaries and the formation of a pollution index. *Helgolander Meeresunters* 33, 566–575. https://doi.org/10.1007/BF02414780

Tsanga A.D., Ekoa Bessa A.Z., Ngueutchoua G., Ngokam G.S., Jacques-David S.M., Ambassa Bela V., Janpou A.K., Abioui M. & Armstrong-Altrin J.S. 2023: Evaluation of provenance and weathering of beach sediments in the lower part of the Cameroonian coast. *Journal of African Earth Sciences* 198, 104822. https://doi.org/10.1016/j.jafrearsci.2022.104822

Verma S.P., Díaz-González L. & Armstrong-Altrin J.S. 2016: Application of a new computer program for tectonic discrimination of Cambrian to Holocene clastic sediments. *Earth Science Informatics* 9, 151–165. https://doi.org/10.1007/s12145-015-0244-0

Verma S.P., Rivera-Gómez M.A., Díaz-González L., Pandarinath K., Amezcua-Valdez A., Rosales-Rivera M., Verma S.K., Quiroz-Ruiz A. & Armstrong-Altrin J.S. 2017: Multidimensional classification of magma types for altered igneous rocks and application to their tectonomagmatic discrimination and igneous provenance of siliciclastic sediments. *Lithos* 278–281, 321–330 https://doi.org/10.1016/j.lithos.2017.02.005

Wang X. & the CGB Sampling Team. 2015: China geochemical baselines: sampling methodology. *Journal of Geochemical Exploration* 148, 25–39. https://doi.org/10.1016/j.gexplo.2014.05.018

Wang, Z., Wang, J., Fu, X., Feng, X., Armstrong-Altrin, J.S., Zhan, W., Wan, Y., Song, C., Ma, L. & Shen, L. 2019: Sedimentary successions and onset of the Mesozoic Qiangtang rift basin (northern Tibet), Southwest China: Insights on the Paleo- and Meso-Tethys evolution. *Marine and Petroleum Geology,* 102, 657–679. https://doi.org/10.1016/j.marpetgeo.2019.01.017

Weber B., Schaaf P., Valencia V.A., Iriondo A. & Ortega-Gutiérrez F. 2006: Provenance ages of Late Paleozoic sandstones (Santa Rosa Formation) from the Maya Block, SE Mexico. Implications on tectonic evolution of western Pangea. *Revista Mexicana de Ciencias Geologicas* 23, 262–276. https://rmcg.geociencias.unam.mx/index.php/rmcg/article/view/816

Weber B., Valencia V.A., Schaaf P., Pompa-Mera V. & Ruiz J. 2008: Significance of Provenance Ages from the Chiapas Massif Complex (Southeastern Mexico): Redefining the Paleozoic basement of the Maya Block and its evolution in a Peri-Gondwanan realm. *Journal of Geology* 116, 619–639. https://doi.org/10.1086/591994

Wiedenbeck M., Hanchar J.M., Peck W.H., Sylvester P., Valley J., Whitehouse M., Kronz A., Morishita Y. & Nasdala L. 1995: Further Characterization of the 91500 zircon crystal. *Geostandards and Geoanalytical Research* 28, 9–39. https://doi.org/10.1111/j.1751-908X.2004.tb01041.x

Windom H.L., Schropp S.J., Calder S.F., Ryan J.D., Smith Jr R.G., Burney L.C., Lewis F.G. & Rawlinson Ch.H. 1989: Natural trace metal concentrations in estuarine and coastal marine sediments of the southeastern United States. *Environmental Science & Technology* 23, 314–320. https://doi.org/10.1021/es00180a008

Wu Q., Nsingi J.M., Kürschner W.M., Beaty B.J., Planavsky N.J., Schneebeli-Hermann E., Yao W., Cepin E.R. & Cui Y. 2025: Impacts of volcanism on geochemical records during the Late Permian-Early Triassic transition in northern and middle Norwegian continental margins. *Global and Planetary Change* 252, 104874. https://doi.org/10.1016/j.gloplacha.2025.104874

Zhao Z., Yin Q. & Sun X. 2025: Detrital zircon geochronology of river sands from the Salween River: Implications for sedimentary provenance and erosion pattern. *Geomorphology* 480, 109754. https://doi.org/10.1016/j.geomorph.2025.109754

Zhou Y., Yang X., Zhang D., Mackenzie L.L. & Chen B. 2021: Sedimentological and geochemical characteristics of sediments and their potential correlations to the processes of desertification along the Keriya River in the Taklamakan Desert, western China. *Geomorphology* 375, 107560. https://doi.org/10.1016/j.geomorph.2020.107560

Zoller W.H., Gladney E.S. & Duce R.A. 1974: Atmosphere concentrations and sources of trace metals at the South Pole. *Science* 183, 199–201. https://doi.org/10.1126/science.183.4121.198

Electronic supplementary material is available online:
https://geologicacarpathica.com/data/files/supplements/GC-77-2-Ramos-Vazquez_Supplement.docx